MICROFLUIDIC CONTINUOUS FLOW IMMUNOASSAY FOR AUTONOMOUS MEASUREMENT OF INFLAMMATION MARKERS IN A NATIVE SAMPLE STREAM

By

LAWRENCE A. SASSO JR.

A Dissertation submitted to the

Graduate School-New Brunswick

Rutgers, The State University of New Jersey

And

The Graduate School of Biomedical Sciences

University of Medicine and Dentistry of New Jersey

in partial fulfillment of the requirements

for the degree of

Doctor of Philosophy

Graduate Program in Biomedical Engineering

written under the direction of

Dr. Jeffrey D. Zahn

and approved by

_____

_____

_____

_____

New Brunswick, New Jersey

May, 2012

ABSTRACT OF THE DISSERTATION

Microfluidic Continuous Flow Immunoassay for Autonomous Measurement of Inflammation Markers in a Native Sample Stream

By LAWRENCE A. SASSO JR.

Dissertation Director:

Dr. Jeffrey D. Zahn

A microfluidic device is presented which fully automates all of the incubation steps of a microbead immunoassay. The device requires only controlled inlet flow rates to achieve this automation, and has no moving parts. These assays are useful for a wide variety of biomolecular quantification applications. Additional benefits of the micro-immunoassay are small sample volume requirements, high sampling rate capability, continuous monitoring, and the potential for real time monitoring of time-varying sample concentrations. The continuous monitoring feature has specific clinical applications such as studying the time course of inflammatory biomarkers in the blood during mechanical circulatory support procedures, and studying the inflammation response in cerebrospinal fluid following spinal cord injury. It has also been shown that multiplexed quantification on a single micro-immunoassay chip is possible. These unique features will enable a variety of new functionalities for clinical diagnostics and laboratory research as compared to existing assay techniques.

PREFACE

Opportunity is missed by most people because it is dressed in overalls and looks like work.

Thomas Alva Edison

We have also come to this hallowed spot to remind America of the fierce urgency of now. This is no time to engage in the luxury of cooling off or to take the tranquilizing drug of gradualism.

Martin Luther King Jr.

The only thing we have to fear is fear itself – nameless, unreasoning, unjustified terror which paralyzes needed efforts to convert retreat into advance.

Franklin Delano Roosevelt

Make it happen.

ACKNOWLEDGEMENT

First, I would like to acknowledge the role of public funding in all of my years as a student (23.5 years in total). I would especially like to thank the people of New Jersey for continuing to support higher education and academic research. Let's strive to make our public education system the best in the country, and to keep New Jersey on top by supporting our highly technical economy and educated workforce.

I would like to thank my advisor, Dr. Jeffrey Zahn, for giving me both the guidance as well as the independence to solve problems and develop this new technology. Additionally, I would like to thank Dr. Zahn and Dr. Ündar for defining the problem and guiding me in the prior art and technical and clinical considerations. Finally, thank you to the committee as a whole for taking the time to understand the project and critically evaluate the work.

I truly appreciate the financial support of fellowships from the New Jersey Commission on Spinal Cord Research, and the Rutgers-UMDNJ Biotechnology Training Program. I am honored and grateful to have been able to participate in the extraordinary educational experience provided by the Biotechnology Training Program. This program succeeds in presenting the student with a thorough, broad, and applicable perspective on the industry.

Grants from the following sources generously supported this project: NIH Heart Lung Blood Institute, the Wallace H. Coulter Foundation, the University of Cincinnati POC-CENT (NIH), Rutgers University Office of VP for Research and Economic Development Proof of Concept Fund.

I would like to thank all of the undergraduate students who helped with various aspects of this project, some of whom were extremely bright and offered significant assistance. The best of luck with your careers.

Finally, I would like to acknowledge the role of risk as an imperative for growth. I am grateful for the bold individuals before me who made sacrifices and took risks in order progress our understanding of the world around us, and to employ this knowledge toward improving our quality of life.

TABLE OF CONTENTS

LIST OF FIGURES

LIST OF EQUATIONS

1 INTRODUCTION

1.1 Motivation

While the immunoassay technology described herein has a wide range of applications, it was developed as a solution to a specific problem. The initial motivation for the work was to provide a clinical functionality which remains unaddressed by any other technology. This initial clinical application was the monitoring of inflammation biomarkers during cardiopulmonary bypass, which was later expanded to include additional mechanical circulatory support procedures. This application presented numerous specific engineering constraints which are detailed in Section 2.2. During the early stages of development, a second application was identified which had similar constraints to the original. This application involved studying the inflammatory response in cerebrospinal fluid following spinal cord injury (SCI). In addition to the technical similarities from an engineering standpoint, both of these applications shared a motivation in that there is currently no other technology which can provide this functionality.

1.1.1 Mechanical circulatory support

The two types of mechanical circulatory support of interest are cardiopulmonary bypass (CPB) and extracorporeal life support (ECLS). While these procedures have some overlap in terms of the equipment which can be applied, there are numerous differences in terms of the health of the patient, the amount of trauma caused by application of the procedure, and other factors which affect the severity of inflammation and the overall

patient outcomes. The details of the procedures and their effects on inflammation will be described in the Background section (Section 2.1.1), with a brief overview of the impact of these procedures given below.

1.1.1.1 Cardiopulmonary bypass

The CPB procedure is used during cardiac surgeries to allow surgeons to operate on a motionless heart. While the procedure is commonly used for adult cardiac surgery, its use during pediatric surgeries adds significant complexity and involves greater risks of long term morbidity due to systemic inflammation. The vast majority of pediatric CPB cardiac surgeries involve repairs of congenital defects, although in some cases surgeons must operate to repair damage caused by disease. Estimates of the prevalence of congenital heart disease vary, with a U.S. study showing around 1 in 150 children born with one of these defects (1), and a Canadian study showing around 1 in 84 (2). While there are numerous defects which are not severe enough to require surgery, around half of these cases would benefit from surgical repairs. Costs related to these disorders are staggering, with about $2.6 billion spent in the U.S. per year for direct hospital expenses (3). While pediatric surgeries involving CPB have a relatively high survival rate, it is the long term complications in these patients which may be mitigated through controlling and reducing systemic inflammation.

1.1.1.2 Extracorporeal life support

ECLS is utilized for both cardiac as well as respiratory dysfunction to assist the cardiovascular system. This may include bridge-to-transplant applications for patients suffering from congestive heart failure or congenital defects, as well as pulmonary

support during illnesses. The mortality rate for ECLS is relatively high, partly due to the nature of the conditions being treated. The mortality rate for neonatal cardiac cases is 61%, while the rate for respiratory cases is 25% (4). The effects of systemic inflammation during ECLS on mortality are not fully understood. A thorough characterization of inflammation biomarkers would help to determine the effects of inflammation on ECLS outcomes, as well as provide information on the efficacy of treatments.

1.1.2 Spinal cord injury

Spinal cord injury is a severe yet common medical condition causing significant impairment to those affected. Over 12,000 new cases of SCI occur each year in the United States, with more than 250,000 people living with this condition. Those suffering injury at a young age require lifelong care with expenses ranging from 1 to over 3 million dollars (5). While research in recent years has shown that nerves have the ability to regenerate, physiological responses inhibit full healing of the nerve injury. The injury response after SCI includes the production of a variety of signaling factors which interfere with the regeneration of nerves across the injury site. This type of injury results in the loss of sensory and motor control. Among the biological responses which inhibit regeneration, one of the least understood is the inflammatory response. The inflammatory response recruits many different cell types to the injury location, including neutrophils, leukocytes, activated microglia, and macrophages which contribute to cytotoxicity following SCI. It can also cause additional damage near the injury site resulting in a glial scar which not only serves to separate injured tissue from healthy, but also creates a physical and chemical barrier to axonal growth and reconnection. Spinal cord injury (SCI) has been shown to induce complex inflammatory responses at the spinal cord

lesion via primary and secondary mechanisms (6). The cell damage caused by this inflammation is one of the significant factors which interferes with nerve regeneration and recovery of motor control. Although the role of this inflammatory response in SCI treatment is not completely understood, specific mediators (e.g. complements and cytokines) are related to axonal demyelination and loss of sensory and motor function. The microfluidic immunoassay presented here is designed to enable characterization of the inflammatory response which is not currently available with other technologies. It is believed that this advanced characterization will lead to improved treatment strategies for spinal cord injury.

1.2 Research objectives

The goal of this research was to develop an autonomous immunoassay which directly measures protein concentrations in a sample stream at high sampling rates and with small sample volumes. In order to address the clinical applications described above, it was intended that the assay would be able to analyze a sample stream drawn directly from an in-vivo source without preliminary modification of the antigen. The design followed the basic assumption that a continuous flow microfluidic system with a fluorescent microbead assay would be an ideal platform. Additional benefits would be gained by incorporating real time measurements, as well as through multiplexing of analytes.

1.3 Hypothesis

Microfluidics lends itself well to the design objectives specifically due to the ability to manipulate small fluid volumes with high accuracy, which is a critical requirement for the identified applications. While autonomous operation is not inherent in microfluidic

devices, and is currently not the standard, an assumption was made that process autonomy could be accomplished with an appropriate design approach. The fluorescent immunoassay platform was chosen because it is an established method for detection of the biological molecules of interest, and the design of a novel assay chemistry was beyond the scope of the project. After thorough consideration of existing microfluidic assay methods, it was determined that a cytometric bead processing device would be a good candidate for the novel design. Previous work in this laboratory with hydrodynamic microbead manipulation exposed intricacies with this method, which led to the decision to use an alternative control scheme relying on magnetism. Examples of this method had been previously reported but not yet thoroughly explored to the point where it would provide the functionality required, however it showed promise in improving the robustness of control over hydrodynamic methods. Based on this exploratory process, it was hypothesized that **a robust, autonomous, high sampling rate quantification assay with specificity toward the inflammatory proteins of interest could be implemented using a novel embodiment of the magnetic microbead manipulation approach**.

1.4 Dissertation organization

The dissertation is organized to outline the research as a traditional engineering project, beginning with the motivation and scientific background, followed by a proof-of-concept based on the initial hypothesis, a redesign stage, and finally an optimization stage. The conclusion includes thoughts for future work on technical enhancements as well as matters related to the final stage of engineering, commercial development.

2 BACKGROUND

2.1 Inflammation

Inflammation is a biological mechanism intended to assist in the removal of infectious and other damaging foreign materials as well as damaged native tissue materials from the body. The inflammation response is an important protective adaptation which also ties into the process of tissue repair (7). Inflammation is characterized by the release of a cascade of proteins and cells leading to a variety of cellular responses in tissues, and ultimately to leukocyte activation and phagocytosis. During phagocytosis, activated leukocytes (white blood cells) destroy foreign materials and infectious agents. They also release microbicidal and other cell-damaging products intended to assist with remediation of the offending substance. These products, as well as other functions of the inflammation response, can also damage normal tissue. While the majority of inflammatory responses are beneficial, treatments for various pathologies are aimed at controlling or interfering with portions of the natural inflammatory response in order to reduce damage to normal tissue and improve prognoses. As the inflammation cascade propagates, its molecular components are present in increasing concentrations in body fluids such blood and CSF.

Inflammation components found in blood plasma and CSF during an inflammation event originate from two sources. Some are normally suspended in the blood and CSF but remain inactivated until the inflammation pathway is activated, and others are derived from cells which are stimulated to release an inflammatory protein, which can either be pre-existing in the cell and simply excreted, or created de novo. Proteins which are pre-

formed tend to be present earlier in the inflammation response, while newly synthesized proteins respond later. Thus, the full inflammatory response involves a multitude of different proteins and cells, performing different or overlapping functions, and presenting with a variety of temporal profiles. This work is focused only on the protein components of the inflammation system which are believed to effectively act as quantifiable markers of the severity of inflammation responses.

All of the proteins of interest function as signals which mediate the inflammatory response. These signaling proteins act in a variety of ways including activation of leukocytes, marking offending particles for destruction by leukocytes, and signaling related to other proteins within the inflammation cascade. The inflammatory markers considered to be assay targets in this work fall in the categories of complements and cytokines.

2.1.1 Mechanical circulatory support and systemic inflammation

The cardiopulmonary bypass procedure is used during many cardiac surgeries so that the heart can remain motionless during surgery, but the body can still be perfused with oxygenated blood to avoid cell death. During CPB, venous blood is withdrawn from the right atrium and pumped through an oxygenator before returning as oxygenated blood to the patient through the ascending thoracic aorta, bypassing the heart and lungs. The heart is arrested once suitable perfusion is achieved, and this state is maintained until the completion of the surgery when the heart is re-started and the CPB circuit is disconnected. A schematic of the CPB circuit is shown in Figure 2-1.

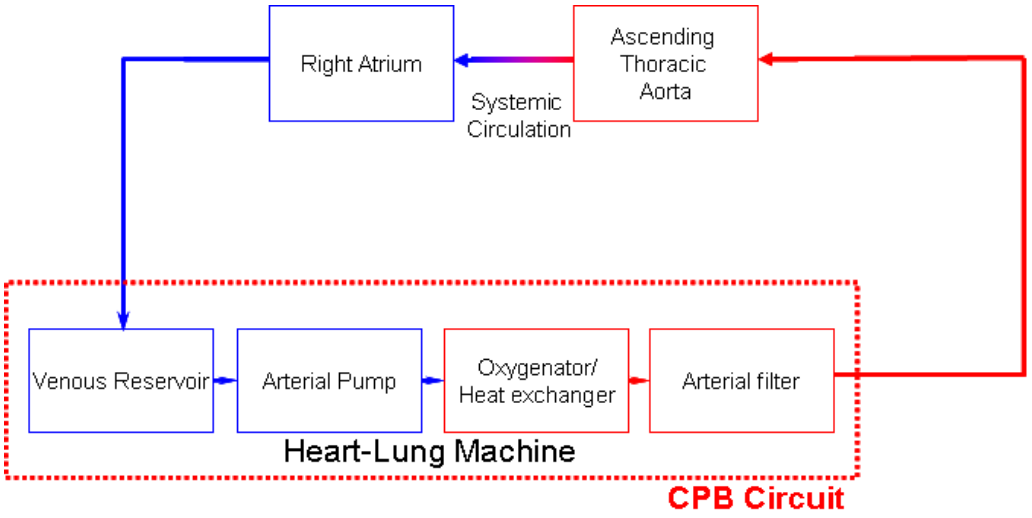

Figure 2-1: Block diagram of the Cardiopulmonary Bypass Circuit (Figure by Akif Ündar)

Cardiac surgeries involving cardiopulmonary bypass (CPB) are known to cause systemic inflammatory responses (8-11). The triggering mechanism of systemic inflammatory syndrome in cardiopulmonary bypass is associated with complement activation (10, 12-15), although contact activation is also involved (12, 14, 16). This activation leads to multiple humoral and cellular inflammatory responses involving neutrophils, platelets, monocytes, mast cells, and endothelial cells. These inflammatory responses are caused by the exposure of blood to the nonphysiologic surfaces of the heart-lung circuit, ischemia-reperfusion of the involved tissues, surgical trauma and hypothermia (10). There are numerous reports detailing the postoperative complications caused by systemic inflammation during CPB. The complications include capillary leak syndrome and vital organ dysfunction that can lead to multi-organ failure and even death (9, 17-19). These complications lead to prolonged hospitalization and increased treatment costs.

The inflammatory mechanisms involved during ECLS are believed to be similar to those involved with CPB. However, the long term nature of ECLS adds additional complications. While CPB is generally applied for hours, ECLS can be applied for days or weeks, and the systemic inflammatory condition may endure and cause organ damage throughout this time. However, some of the causes of inflammation may be mitigated by the fact that the heart is not stopped and the lungs are not bypassed during ECLS, reducing the surgical trauma and some of the direct causes of inflammation. Only a thorough characterization of the various inflammatory markers will enable a determination of the causes and mitigating factors for inflammation during mechanical circulatory support procedures.

2.1.1.1 Assessing inflammation during mechanical circulatory support

It has thus far been difficult to thoroughly study the inflammation process during mechanical circulatory support procedures due to the lack of data regarding inflammatory responses. While studies have been done to measure some of the inflammatory markers during and after cardiac surgeries involving CPB, these studies have had very low sampling rates with sample periods of 1 hour or more over a total monitoring period of 24 to 48 hours (10). While this type of data is important to the study of systemic inflammation, it is mostly useful in understanding postoperative recovery, and lacks the detail required to pinpoint the onset of inflammation, and the significance of each inflammatory marker at different times during and after the surgery. Other studies have focused on achieving higher sampling rates, but these studies have only been conducted on simulated CPB circuits (20). While the sample intervals in these studies have been as low as 15 minutes, it is difficult to realize sampling rates this high during actual patient

surgeries due to the large total amount of blood that must be drawn for a large number of samples.

Conventional assays that measure protein concentration, such as the enzyme linked immunosorbent assay (ELISA) and immunofluorocytometry, typically require a minimum of 50 to 100 µl of blood per sample. Due to limitations on the amount of blood that can be drawn from a patient during cardiac surgeries, and the feasibility of successive analysis of large numbers of samples, these assays are not conducive to time course studies with many samples over the course of four or more hours. This problem is exacerbated in the case of surgeries on neonates, since the total blood volume of a 3 kg neonate is only 240 ml. The large sample volumes and low sampling rates of existing assays for measuring the concentration of inflammation markers found in the blood during CPB has been a limiting factor in the study of the systemic inflammation process.

Partly due to the inability to thoroughly monitor and study inflammation, no universally effective set of treatments currently exists to mitigate the inflammatory response to CPB and ECLS. Patients would ultimately benefit from novel treatment approaches meant to reduce inflammation, as well as modifications to the circuits and surgical techniques. However, developments in this area have been slow due to the lack of characterization of the inflammatory response. Continuous monitoring of inflammation during these procedures would offer numerous advantages to researchers and clinicians. The real-time data will allow the surgical team to determine whether increases in inflammation are a direct result of specific aspects of the surgery. As these factors are added to the general knowledgebase, surgical teams could begin making adjustments during the surgery such as anesthetic substitution, more aggressive plasma ultra-filtration

during postoperative hemoconcentration, as well as substitution of other pharmacological agents which have been shown to affect total inflammation and outcomes (20-26). This technology would also significantly improve the quality of clinical research on the effects of different CPB and ECLS equipment and perfusion-related parameters. Thus, an assay that can provide these measurements at high sampling rates using very small volumes of blood would be a valuable research and clinical tool.

2.1.2 Inflammatory response to spinal cord injury

The triggering mechanism of inflammatory responses following SCI is associated with the recruitment of immune cells. These inflammatory cells are important contributors to secondary damage following SCI, including neutrophils, leukocytes, activated microglia, macrophages and T lymphocytes (27, 28). These inflammatory cells are associated with spinal cord scarring, axonal demyelination, and neuronal death, but may also be integral for chronic neuroregeneration. These cells, particularly microglia and macrophages, contribute to cytotoxicity following SCI, particularly within the wound core (29-32). Another end-product of the inflammatory response is the glial scar. The glial scar is formed primarily by astrocytes that are activated by molecules at the injury site. While the glial scar serves to separate injured tissue from healthy, unfortunately, it also creates a physical and chemical barrier to axonal growth and reconnection (33).

To control inflammation following acute SCI, several studies have demonstrated the beneficial effects of methylprednisolone infusion following injury (34). Patients treated within eight hours of injury with methylprednisolone showed significant improvement in sensory and motor functions compared to those who did not receive treatment. Currently, methylprednisolone is given intravenously at a dose of 30 mg/kg over 15 minutes

followed after 45 minutes by 5.4 mg/kg/hr for 23 hours. Although methylprednisolone is commonly used to treat acute SCI, other treatments are under investigation and must be carefully evaluated. For example, the use of erythropoietin has shown some promise in reducing secondary injury. However, it has been shown that methylprednisolone and erythropoietin do not act synergistically, and that co-administration of methylprednisolone and erythropoietin removed the beneficial effects of using erythropoietin in a rat model (35). Other research examining the use of 4-aminopyridine (4-AP) has shown infusion regimen specific outcomes. For example, work at Baylor College of Medicine has demonstrated that intravenous infusion of 4-AP showed no short term benefits in restoration of motor control (36) while intrathecal administration may have benefits (37). These studies demonstrate the importance of monitoring complement and cytokine levels to understand the inflammation mechanisms in patients following SCI, and that these inflammation markers may indicate the use of appropriate therapeutic targets to minimize secondary damage and retain locomotor function following SCI. These results suggest that well controlled studies, with real time monitoring of inflammation markers will allow the clinical team treating the spinal damage to determine any significant changes in inflammation as soon as they occur. Online measurements of inflammation would permit studies of the effects of different pharmacological agents, equipment and procedures.

2.2 Novel assay constraints and goals

An assay capable of thoroughly characterizing inflammatory responses would be beneficial to the study and treatment of both inflammation caused by mechanical circulatory support, as well as inflammation occurring subsequent to spinal cord injury.

There are specific constraints which must be met in order for the assay to be adequate for these applications. A discussion of these constraints follows.

2.2.1 Assay targets

Complement C3a is one of the most important inflammatory markers related to CPB due to its relevance to the pathways which are activated resulting in the generation of the membrane attack complex which can cause cell and tissue damage. This molecule is also found at relatively high concentrations in the blood. It has been shown in multiple studies that C3a concentrations increase considerably once CPB has begun (11, 38). Complement C5a activation has also been shown to result from CPB (11). Along with these complements, various cytokines have been implicated as significant markers of systemic inflammation during CPB. Specifically, TNFα and interleukins IL-1, IL-6 and IL-8 are important signaling factors for systemic inflammatory responses (39). Complement C3 is also activated following spinal cord injury (40, 41). IL-1, IL-6 and TNFα have also been shown to be important markers for inflammation related to SCI (42), as well as PGE_2 (43). Thus, these complements and cytokines will be the targets for the novel assay, with complement C3a being the most significant and first to be tested.

2.2.2 Sample volume consumption

The primary restriction on assaying for both blood plasma and CSF relates to the overall fluid volume consumed during the entire assay. The fluid volume consumption depends on different factors depending on the type of assay used. Two applicable assay types have been identified in terms of the method of fluid consumption. Specifically, there is a discrete batch method, and a continuous flow method. These methods of sample

fluid consumption do not necessarily correlate with discrete versus continuous sampling, which is related to when and how measurements are recorded. The volume of sample fluid consumed in a discrete batch assay equals the discrete sample volume multiplied by the total number of samples taken. The rate of consumption thus equals the discrete sample volume multiplied by sampling rate. In contrast, for continuous flow assays the total volume consumed is simply equal to the sample flow rate multiplied by the total assay time. None of the traditional or novel assays considered for this application require significantly large volumes of sample fluid for the sensing method to function. The requirement of relatively large sample volumes with traditional assays inevitably arises due to limitations of the fluid handling techniques.

The maximum assay sample consumption volumes for blood plasma and CSF are not entirely defined, however it is clear that many common assays would require far too much sample volume for repeated measurements. Patients undergoing cardiac surgeries involving mechanical circulatory support are already at risk for blood loss and blood damage, and therefore further loss of blood to assaying is very restricted. This problem is exacerbated in the case of pediatric and neonatal patients, where total blood volume is much lower than for adult patients. The worst case scenario is that of a 3 kg neonate, where the total blood volume is only 240 ml. To account for the worst case condition for CPB applications, a total sample consumption limit of 10 ml will be specified for the full assay duration.

For the case of CSF monitoring, different criteria apply. An animal model using rats will be required for benchmarking of the assay, and because rats have significantly lower volumes of CSF than humans, the sample consumption will be specified based on the rat

model. An adult rat weighing 300 g has approximately 580 µl of CSF (44). It has been reported that 50 to 150 µl of CSF can be sampled at one time from an adult rat without signs of disturbing the animal (45). While total CSF volumes are rather low compared to the total blood volume of the same animal, CSF has the benefit of a relatively high rate of replacement. A recent study showed that adult rat CSF is produced at a rate between 1.8 and 2.5 µl/min, depending on age (46). Thus, recovery from a 50 µl sample should require no more than 28 minutes, assuming a 1.8 µl/min CSF production rate. Based on these assumptions, a maximum total CSF volume is not required, and a maximum discrete batch sampling rate of 50 µl each half hour can be specified. Alternatively, for a continuous flow assay, a maximum sample flow rate of 1.8 µl/min can be specified.

2.2.3 Assay measurement lag time

The lag time of the assay is defined as the elapsed time from the point when the measurement is desired to the point when that measurement value is provided. For any study, the lag time depends on the characteristics of the assay used, as well as the implementation. For many traditional assays which use discrete batch sampling, the samples are frozen for a period of time before they are assayed. In these cases, the assay may have a minimum lag time equal to the assay time if performed immediately after sample collection (often around 3 hours), but the actual implementation generally involves freezing the samples for days or weeks, resulting in an assay lag time of days or weeks. It is often the case that a particular assay could theoretically be performed on-the-fly to provide shorter lag time, but it is usually unreasonable to do so in terms of cost, equipment, and personnel requirements. Alternatively, for a continuous flow assay, the lag time depends on the specific mode of operation of the device. Generally there is some

finite amount of time taken for the assay to occur once the sample reaches the device. There is also a delay in sample delivery since the sample fluid must be carried to the device from the subject through tubing. An assay with a relatively short lag time offers the added benefit real-time monitoring and the potential for personalized treatment. Thus, for both CPB and SCI assays, the goal will be to provide a lag time as close as possible to the assay time, since assay time is the limiting factor. This will be accomplished by reducing the swept fluid volume of the tubing and interconnects as much as possible, and using the highest flow rates possible in these components without passing the volume consumption limit.

2.2.4 Measurement sampling rate

The sampling rate of the assay determines how thoroughly the target system can be characterized. The maximum feasible sampling rate depends on the type of assay used, the sample volume limitations, and the specific implementation. For measurement of physiological blood inflammation during CPB, only discrete batch assays have been reported in the literature. Inflammation studies for adult CPB patients have used sampling intervals in the range of multiple hours (11, 38), however the sample volumes for these studies are generally in the range of 1 to 5 ml per sample, which is somewhat greater than the minimum volume for the fluid handling techniques and assays methods used. Advanced time-course inflammation studies on pseudo-patient CPB setups have shown best case sample intervals of 15 minutes, but this sampling rate is sustained for a much shorter duration than is required for a CPB procedure, and the blood volume consumption is well beyond the maximum allowed.

Inflammation measurements from spinal cord injury studies tend to use discrete, low sampling rate assays. Most animal model studies of inflammation following spinal cord trauma use sample intervals of an hour or greater (40-42, 47, 48). A microdialysis study was conducted which measured PGE_2 following intrathecal administration of IL-1β to temporally track the changes in PGE_2 levels in the CSF (43). The results show variation in concentration of PGE_2 by as much as 3 times within a 30 minute sample interval. While the physiological relevance of this response is unknown, it shows that portions of the inflammatory pathway can respond at rates much higher than what is being measured in most studies.

In order to make a significant impact on the ability to track blood and CSF inflammation markers, the ultimate goal for the sample interval is 5 minutes or less. For discrete batch assays, the sampling rate is defined as the number of times per hour that the sample fluid is drawn and collected. Thus, for a discrete batch assay this requires a fluid sample to be collected every 5 minutes. It is assumed that no dataset filtering is used for this case. For continuous flow assays, the sampling rate can be more difficult to define due to the use of a moving average, or finite impulse response (FIR) filter to reduce measurement noise. To take a worst case scenario for a moving average filtered dataset, the sample interval can be assumed equal to the filter window size. For a continuous flow assay, the moving average filter window must not be wider than 5 minutes while maintaining acceptable assay noise. When the filter window is shortened, the noise in the dataset increases, however the transient response improves. It is assumed that an FIR filter with a 5 minute window will not slow the transient response of the assay to a point where it can not accurately indicate physiological changes in the blood or

CSF levels of inflammatory markers. This cannot currently be tested because no assay exists that can sample in vivo blood or CSF protein levels quickly enough to show the maximum rate of change. Due to limitations on the equipment available for the novel assay, initial experiments will likely have sample intervals of 15 minutes, which is considered to be a large improvement over most traditional assays.

2.2.5 Assay duration

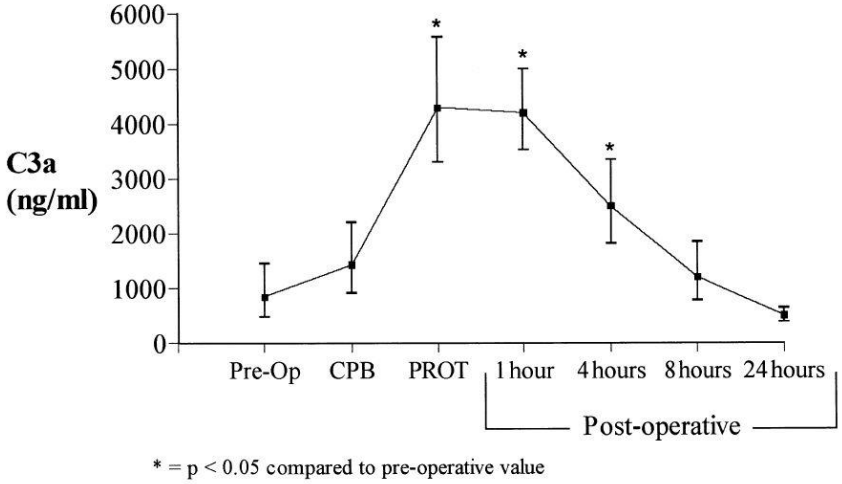

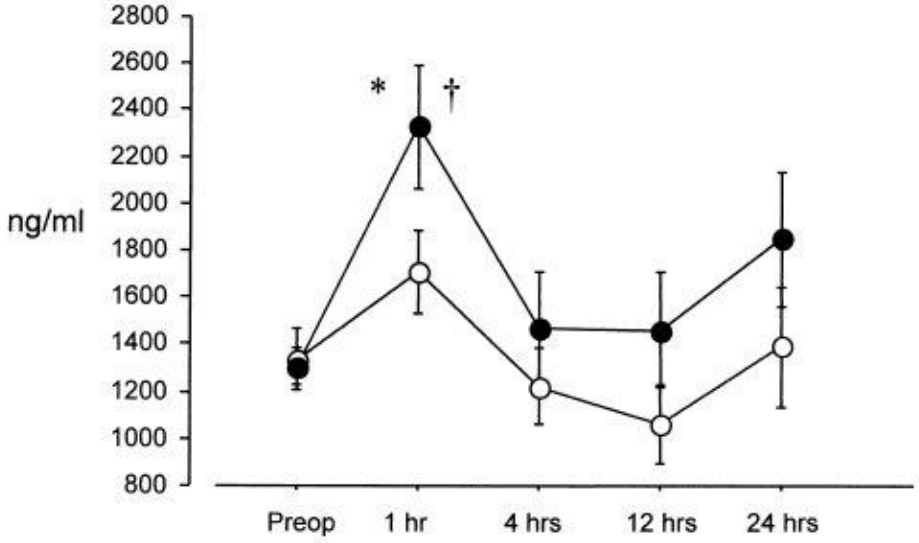

Figure 2-2: (Top) Changes in activated complement C3 (C3a) levels in 16 patients undergoing modified Fontan procedure. (CPB = cardiopulmonary bypass; Pre-Op = preoperative; PROT = protamine administration). (Mainwaring et al., 1998)

(Bottom) Changes in C3a concentrations for patients undergoing coronary artery bypass grafting. Preoperative and 1, 4, 12, and 24 hours postoperative. (Filled circles) On-pump group (n = 30); (open circles) off-pump group (n = 30). (Ascione et al., 2000)

Considering Figure 2-2 showing complement C3a concentration versus time during and after CPB procedures from two studies (11, 38), there is one area of the plot which clearly fails to provide an adequate sampling rate. The area between the start of the CPB procedure and the administration of protamine at the end of surgery shows a very high rate of increase in the C3a concentration. Protamine is given to reverse the effects of anticoagulation therapy needed during surgery. Thus, in this study there are no data points between the beginning of surgery and the end of surgery. It would be most beneficial to further characterize the inflammation response during this period of time. Generally, cardiac surgeries with CPB are completed in 2 to 4 hours, thus a 4 hour minimum assay duration is required.

For SCI inflammation studies, as well as for longer term extracorporeal circulation (such as extra corporeal life support), a longer duration of sensing will be required. One study showed elevated levels of IL-1β in CSF 7 days after spinal cord injury (42). Thus, while initial experiments will aim for a 4 hour duration, long term development will aim toward assay durations of 1 week or more. Re-calibration may or may not be required during these long term experiments due to drift in the intensity of the fluorescent tag or other unknown variables.

2.2.6 In-vitro complement activation

Common assay protocols for protein samples allow for sample storage either refrigerated at 4° C for short periods of time, or frozen for extended periods of time. Typically, the only source of assay inaccuracy caused by storage would be due to small amounts of protein denaturation which occur during freeze-thaw cycles, or over time when the sample is at room temperature preceding an assay. Sample storage for

complement proteins, however, is more complicated since the pathways of compliment activation can continue to function ex-vivo. This process occurs most readily with complement C3, one of the most important parts of the complement system for inflammation monitoring. When inflammation is present, complement C3 that is already present in the affected region is broken down by a C3 convertase called C3bBb (7). Consequently, two fragments are released by the reaction. C3b fixes to a surface (such as a bacterial cell wall) to signal for phagocytosis by neutrophils and macrophages. The second component is the anaphylatoxin C3a, which diffuses away from the site. While C3a is a good marker of inflammation due its release from each potential phagocytosis site, its concentration in a sample unfortunately is not always stable. This problem occurs because the C3 convertase is still present and active in the sample, and it continues to cleave the C3a component from the C3 present in the sample. It is common practice to add the metal chelator ethylenediaminetetraacetic acid (EDTA) to samples, because it is believed to block the functioning of the major pathways of complement activation (49). In a study by Hugli et al. it was shown that after 60 minutes at room temperature C3a concentrations in EDTA samples from normal patients tend to remain stable (50). However, in the same study it was shown that samples handled in the same way from liver transplant patients show an increase in C3a concentration of around 700% after 60 minutes. For these patients it is expected that acute inflammation is present, and while their basal C3a concentrations are notably higher than normal subjects, it is apparent that in-vitro convertase activity in their blood samples is much greater as well.

The addition of the protease inhibitor Futhan (6-amidino-2-naphthyl p-guanidinobenzoate dimethanesulfonate) to the samples can be used to further reduce in-

vitro complement activation. Hugli shows a significant stabilizing effect for room temperature C3a sample concentration with the addition of this compound to plasma samples from liver transplant patients (50). Nonetheless, even with Futhan and EDTA in the samples, an average increase in complement C3a concentration of 25% (from 1.6 µg/ml to 2 µg/ml) is evident after 1 hour at room temperature. This increase in activated C3 over time is not mitigated through application of the assay standard curve, which is used in all applicable assays for calibration, because the standards include only isolated C3a, so no further C3 activation will occur. The issue of in-vitro complement activation at room temperature is especially problematic for traditional bench-top assays since they generally require first stage incubation times of 1 to 2 hours at room temperature, during which time the amount of continued activation of C3 is unknown. Also troublesome is the inconsistency in the amount of in-vitro compliment activation between samples from different patients. Hugli showed that there is a considerable difference when comparing patients with expected acute inflammation versus patients not expected to be experiencing inflammation. Since inflammation is both the target of the assay and a factor contributing to its accuracy, the assay results become unpredictable.

While measures such as the addition of Futhan and careful handling techniques can lead to reasonable accuracy for complement component assays, there is a clear potential benefit to completing the entire assay within minutes after the sample fluid exits the body in order to improve the accuracy and predictability of the assay. While this feature is not specified as a requirement for the novel assay, it could prove to be a significant added benefit to a design which allows continuous flow operation for a native sample stream and performs its primary incubation in a relatively short period of time. It may also

increase the applicability of the assay since this feature offers benefits over traditional assays even for discrete measurements when continuous long-term measurements are not needed.

2.3 Microfluidic assays applicable to inflammatory markers

2.3.1 Overview of relevant microfluidic assays

Microfluidic devices have been developed which are analogous to traditional immunoassays, but offer benefits such as higher throughput and smaller required sample and reagent volumes due to microchip integration (51-53). Many of these devices use optical detection schemes based on fluorescent tags (53), or chemiluminescent reactions using horseradish peroxidase (54, 55). Other microfluidic biosensor designs have replaced these optical detection schemes with electrochemical detection schemes based on impedance or current measurements (56, 57). These microfluidic detection technologies have resulted in immunoassays with higher throughput and significantly increased sensitivity. Although they use reduced sample volumes as compared to traditional methods, these devices were designed as discrete-sample assays. For applications where the analyte concentration is not time-varying in the short term, such as in the detection of protein markers indicative of disease (52) or environmental toxins (54), these assay technologies are effective. However, in applications where the analyte concentration is changing with time and must be analyzed repeatedly these assays must be processed successively, which limits their feasibility for high sampling rate monitoring.

Other technologies have been implemented with the goal of real-time, continuous or semi-continuous biosensing. A design by Engstrom et al. (58) was able to monitor the

concentration of carbohydrates in a sample stream at a very high sampling rate, taking one sample every second, as shown in Figure 2-3.

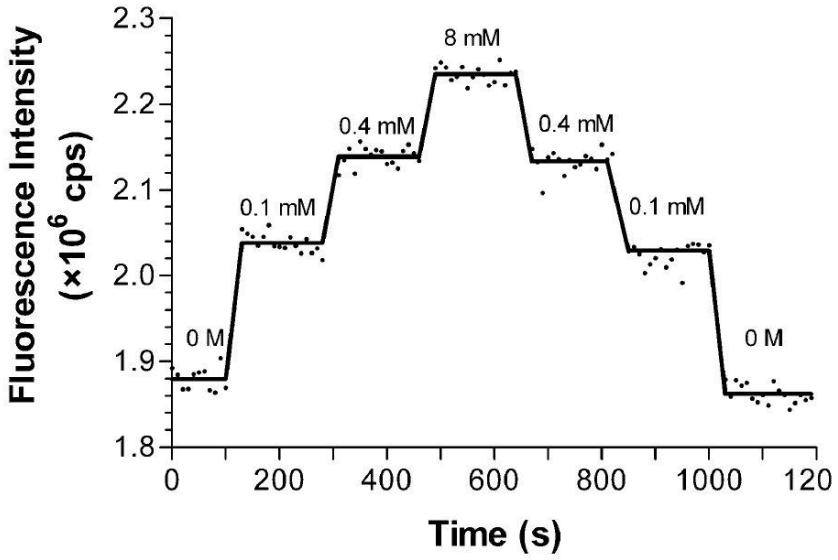

Figure 2-3: Fluorescence response to step wise injections of maltose at varying concentrations. Lines represent mean values for each injection. (Engstrom et al., 2005)

Measurements were purely optical, based on total internal reflection fluorescence, allowing direct measurement of the carbohydrate sample without a separate labeling phase. The detection system used the intrinsic change in the autofluorescence intensity of the carbohydrate binding antibody's tryptophan residues at 295 nm excitation wavelength upon carbohydrate binding to produce an increase in fluorescence emission. However, the flow rate used for the immunoassay was rather high at 250 μl/min, potentially leading to rapid depletion of the sample fluid. Other groups have developed pseudo real-time integrating sensors based on electrochemical (59) or fluorescent (60) detection. Integrating assays continuously accumulate the analyte, and their direct output is a measure of the total amount of analyte accumulated.

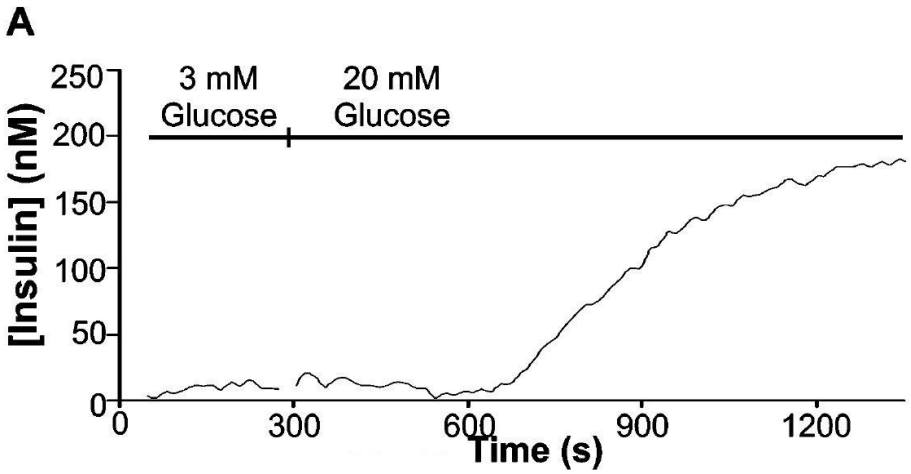

Figure 2-4: Representative plots for integrating real time glucose sensor. (Roper et al., 2003)

The instantaneous sample concentration at any time during the assay is determined based on the rate of change of the sensor's output. While these assays can have very high sensitivities, they are limited in terms of assay duration due to saturation of the sensing element. They can also be prone to drift due to nonlinearities of the sensing element relative to the total amount of accumulated analyte on the sensor.

2.3.2 Continuous flow micro-immunosensor with hydrodynamic actuation

The micro-immunoassay design present builds upon previous work in which streptavidin-biotin binding was used as a model for antibody-antigen interactions (61). In this model, streptavidin-coated microbeads are incubated with a fluorescein fluorescently tagged biotin (biotin-FITC) solution within the microdevice. The incubation time is controlled such that the number of biotin molecules bound to the bead surface is dependent on the concentration of biotin in the sample stream. Since the biotin is already labeled with a fluorescent tag, the streptavidin-biotin binding assays are efficient as

benchmarking studies, requiring only a single bead incubation step. The sample concentration is determined based on the fluorescence intensity of the beads following incubation. Such a microdevice must be capable of reliably manipulating the microbeads, in an autonomous fashion, into and out of the sample stream. This requires the trajectory of the bead to be decoupled from the background carrier flow. In earlier work, the decoupling of bead motion was accomplished through an implementation of microscale hydrodynamics (61) by controlling particle movement at a bifurcating region. While this design proved capable of transferring the beads between adjacent fluid streams, reliability was a problem since the device required precisely tuned flow rates to ensure proper bead trajectories. The design also required very low flow to allow sufficient incubation times. Lower flow rates tend to introduce complications in bead processing due to bead settling and sticking. The purely hydrodynamic design has been replaced with a magnetically actuated control scheme. The magnetic design has proven to be more robust than the hydrodynamic one, leading to a less complicated channel design with much simpler tuning.

2.3.3 Microdevice assays with magnetic microbeads

While many types of assays are capable of protein concentration measurement, many are not easily applied to autonomous measurement of protein concentrations with high sampling rates, low sample usage, and extended measurement durations. Certain magnetic bead based assays do lend themselves to this type of application. Magnetic actuation has been applied in various forms within microfluidic devices (62), but immunoassay devices utilizing magnetic fields tend to employ microbeads. Bead-based micro-immunoassay devices must include some sort of separation method to control the

bead incubation process. For magnetic bead assays, these separation schemes generally fall into two categories. First, in bead trapping devices, the beads are held stationary via a magnetic force while the fluids are manipulated around the beads for the incubation and washing steps. Immunoassays using bead trapping schemes inherently provide batch measurements and are not easily applied to high sampling rate monitoring without complex external fluidic controls, which result in lower sampling rates (63-65). The second type of separation scheme used in magnetic bead based micro-immunoassays is continuous flow operation. In these cases the fluids containing different bead processing reagents are introduced into the device as steady streams, and the beads are magnetically manipulated to move between the streams. Variations of this basic flow manipulation have previously been shown to be applicable to micro-immunoassays. Park and colleagues presented a magnetic based detection scheme where antibody conjugated magnetic nanoparticles were used as the secondary label in an antigen sandwich immunoassay (66). However, the device did not have an integrated incubation control scheme, and was not capable of analyte detection from a native sample stream. For detection of such samples, a multiple step on-chip incubation scheme can be used to enable an antigen sandwich immunoassay. In the design by Pamme and colleagues, a series of coplanar flows within a common channel provides this type of incubation (66). By pulling paramagnetic beads across the wide channel, perpendicularly to the stratified flow environments, the beads pass through a series of incubation and wash streams (Figure 2-5). The incubation time in this device depends on the flow rate as well as the magnetic field intensity, and is limited by both the stream width as well as the transverse bead velocity.

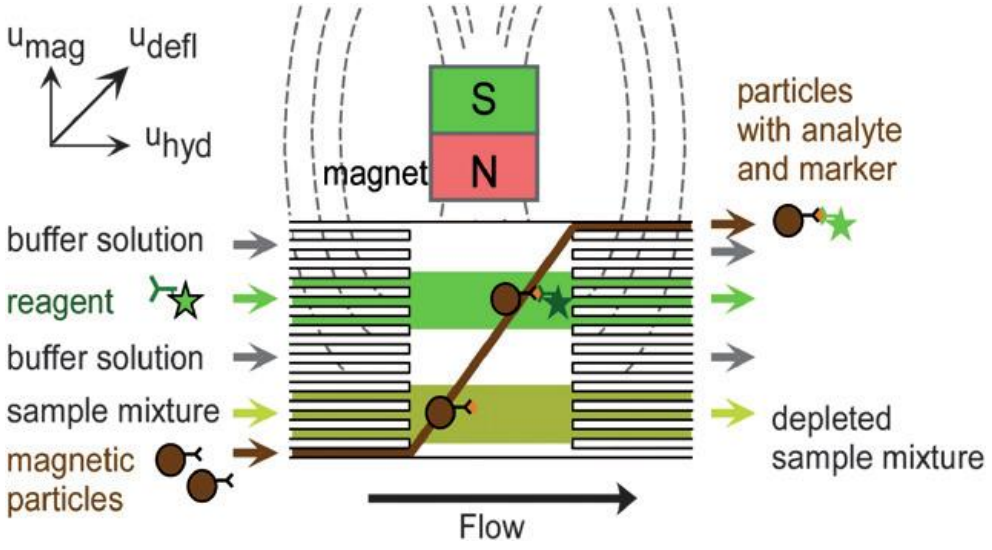

Figure 2-5: Basic magnetically actuated micro-immunoassay design with coplanar flows (Pamme et al., 2009)

2.3.4 Magnetically actuated micro-immunoassay proof of concept design

In contrast to the magnetic actuation scheme shown in Figure 2-5, where beads are incubated while transferring across the channel through stratified environments in a single bead actuation event, it is also possible to arrange multiple bead actuation events on a chip. While making the microfluidic geometry more complex, these separate magnetic actuation events allow much greater control of bead incubation times. This control scheme is the essence of this design. The basic assumptions which led to this choice of design are the tunability of incubation times, the possibility of relatively long incubation times, and the robustness of control. The fundamental features of the novel assay are autonomous on-chip processing of a fluorescence-based sandwich immunoassay carried out with magnetic microbeads, followed by fluorescence detection.

Two implementation techniques have been identified for the magnetically actuated incubations. Both methods relay on the same actuation principle: the bead carrier stream flows adjacent to the incubation stream, where the incubation stream is against the edge of the common microchannel. An external permanent magnet pulls the beads to the edge of the channel where they roll along the wall carried by the incubation stream. This system provides an extremely robust separation technique where the incidence of correct bead transfer can easily be 100%. Once the beads are in the incubation stream, two different incubation methods are possible.

In one incubation method, the magnetic field holds the magnets at the edge of the channel as they progress downstream with the incubation fluid. This case uses magnets that are placed on both sides of a microchannel so that the bead incubations occur along the walls of the channel. The microbeads incubate while rolling along the sidewall of the main channel. The magnetic field is strong enough to pull the beads to the sidewall, but not strong enough to trap them due to the shear stress around the bead from the pressure driven flow. Due to the pressure driven flow in the microdevice and the resulting no-slip boundary condition, the flow outside of the sidewall boundary layer has the highest velocity, and the flow velocity at the wall is near zero. Because the beads are constrained against the channel wall, where the fluid velocity is much lower than towards the center of the channel, they move through the device at a velocity which is significantly slower than the average flow velocity, at 16.5% of the vertical centerline velocity. This effect greatly increases the residence time of the beads in the sample stream relative to the flow rate, achieving much longer incubation times and thus higher sensitivity than a design where the bead incubation occurs while the beads are at a position farther away from the

channel walls. Since the mean antigen stream velocity is also significantly higher than the bead velocity, this arrangement also helps replenish analyte around the bead since the analyte is convectively transported to the surface of the bead not in contact with the sidewall, speeding the incubation process. This design is also critical to the accuracy of the micro-immunoassay because it forces every bead to travel through the microchannel at the same velocity, resulting in identical incubation times and minimizing bead-to-bead variations.

The second incubation method relies on more complex channel geometry to achieve a very long length for the incubation channel. In this method, after the beads are pulled into the sample stream the stream is directed into a long incubation channel. After the initial actuation region, the beads do not remain against the wall. However, the incubation flow splits off from the common channel such that only the sample stream flows into the incubation region of the device. While this design adds complexity to the design and could reduce the uniformity of bead incubation times, it offers a much longer incubation channel for the same overall chip size, which allows increased incubation times as well as increased flow rates for greater flow stability. The incubation channel outlet feeds a common channel where further bead actuation can occur for multiple incubations, and ultimately the beads directed to the detection channel. Another benefit of this design is that it requires only one magnet for the entire assay, whereas the straight channel design requires two magnets per incubation (4 magnets for the complete two-stage sandwich immunoassay), however it requires multiple device layers for multiple incubation stages which adds to fabrication complexity.

3 PROOF OF CONCEPT MICROFLUIDIC IMMUNOASSAY

This novel technology is intended to measure inflammation in a biological sample stream based on known inflammation markers. The original motivating applications identified for this technology involve the same biological markers, which results in a large amount of overlap in the development of the assay for the two applications. Thus, the development of the biochemical aspects of the assay has not been split into application-specific solutions. Furthermore, the microfluidic portion of the assay has remained identical for the two applications. Therefore, the main thrusts of the earlier phases of the research did not required separate consideration for each application. In a later research phase, a small amount of separate consideration regarding the method of sample acquisition from the in-vivo source is required.

3.1 Overview of immunoassay development

The microfluidic immunoassay design is based on continuous incubation of paramagnetic microbeads in a microchannel. A single incubation assay was used to test the hypothesis of the magnetically actuated micro-immunoassay, and for development of the physical parameters of the device. This assay used streptavidin-biotin binding as a model for antibody-antigen binding. Through experimentation, and from reports in the literature, it was determined that streptavidin-biotin binding would be an acceptable model for antibody-antigen interaction when scaled appropriately for binding kinetics. While the model cannot inform the appropriate incubation time for a dual incubation immunoassay, it can assess all aspects of the microdevice kinetics and the detection

scheme. This model has been utilized at various points in the research to test assay design hypotheses without the cost and complexity of the full immunoassay.

For autonomous detection of an untagged protein in a biological sample such as blood plasma or CSF, at least two incubation steps are required to complete an antigen sandwich immunoassay. In the first stage, antibody coated microbeads are incubated with the sample fluid to bind the antigen of interest. In the second stage, the beads are incubated with a fluorescently labeled secondary antibody also specific to the antigen of interest. There are also assays in which a third incubation stage is enlisted to perform the fluorescent tagging, which will be discussed in detail in a later section. In this work two compatible monoclonal antibodies were used in a two-stage operating mode, with each antibody binding a different epitope on the antigen of interest. The result of the bead processing is that subsequent to the two serial incubation steps the beads are coated with the fluorescent tag in an amount that is proportional to the concentration of the antigen in the sample stream. A concentration measurement is made by detecting the fluorescence intensity of each bead after the second incubation stage and comparing the fluorescence intensity to a previously determined calibration curve.

After validating the operating principles of the microdevice with the single stage model, a dual incubation microdevice was validated using bench-top incubations. The dual incubation device was designed based on this validation. The following sections detail the steps taken to design the microfluidic immunoassay.

3.2 Assay design

3.2.1 Single incubation assay bench-top validation

Bench-top incubations were used to determine the appropriate analyte concentration range for the single stage assay, assuming an incubation time of 30 seconds. The incubation time was chosen based on preliminary research which showed it to be within the range achievable with a simple microdevice incubation channel. The microbeads used in these experiments, and throughout this work, are 8 μm diameter, streptavidin-coated, polystyrene beads containing a 1 μm diameter iron oxide paramagnetic core (Bang's Laboratories, Inc., Fisher, IN). 25 μl aliquots of these beads ware washed twice in PBS in Eppendorf tubes (add 1 ml of PBS, vortex, centrifuge). After aspirating, 100 μl analyte samples at varying concentrations were added to the tubes and incubated for 30 seconds. The analyte was a fluorescein conjugated biotin molecule (biotin-FITC) (Invitrogen, Carlsbad, CA, B-10570) which was serially diluted. Incubation was ended by adding 1 ml of PBS, vortexing and centrifuging. The incubated beads were ultimately suspended in 500 μl of PBS.

3.2.2 Single incubation bench-top experimental results

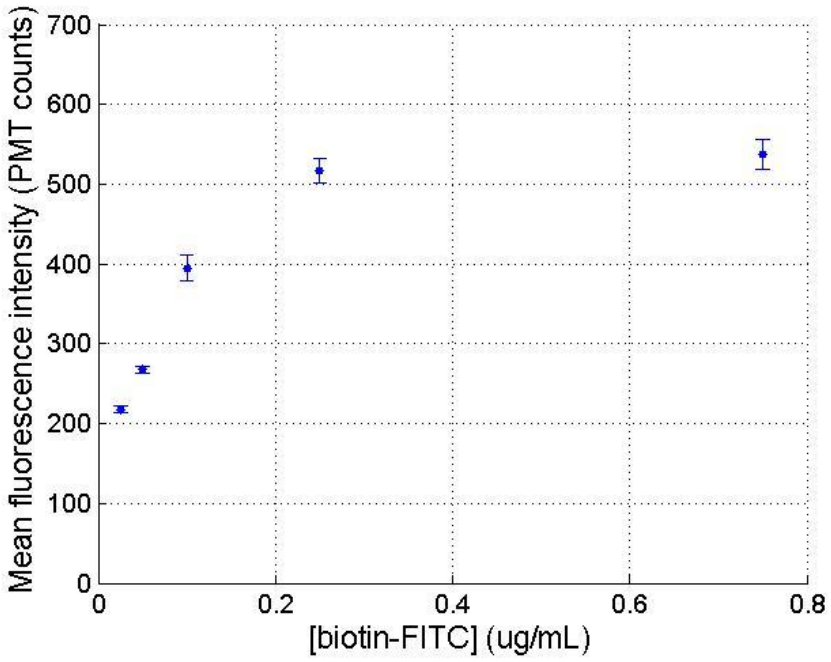

Figure 3-1: Mean fluorescence intensity versus biotin-FITC concentration response curve from microdevice detection following bench-top incubation for 30 seconds to study streptavidin-biotin binding over an extended concentration range. Bead fluorescence saturation is evident at biotin-FITC concentrations higher than 300 ng/ml

Figure 3-1 shows a calibration curve of bead fluorescence versus concentration for streptavidin-biotin binding over an extended concentration range. This data was obtained by the bench-top incubation of the beads with a biotin-FITC solution of known concentration. Following incubation, the beads were resuspended and run through a microchannel for fluorescence detection using an argon ion laser and photomultiplier tube (PMT), described in detail in section 3.4. These data show that there is a linear response region where bead fluorescence intensity is proportional to the biotin-FITC concentration, and a saturation region at higher solution concentrations. In order to

provide meaningful data, the incubation time of the microdevice must be tuned for the expected concentration range so that the beads are not saturated at the highest concentration tested. Bench-top experiments such as this one were used as a simple method to determine the required incubation times in order to design the microchannel incubation length and appropriate syringe pump flow rates for the microdevice assay.

3.2.3 Dual incubation immunoassay bench-top validation

Two additional bench-top incubation experiments were performed during development of the dual incubation micro-immunoassay. These experiments tested the suitability of the microscopy-based fluorescence detection scheme, and the hypothesis that a short incubation with high concentration samples would yield similar total binding to a long incubation with low concentration samples. Both of these experiments were based on a commercially available Cytometric Bead Array Human Anaphylatoxin Kit (BD Biosciences, San Jose, CA, USA). The components used in the novel dual incubation microimmunoassay are similar to those in the commercially available immunofluorocytometry bead assay kit. However, the beads used for this microimmunoassay are paramagnetic, which is required for the autonomous processing within the microdevice. This assay also differs from the commercially available kits in that it is intended to directly measure samples at systemic antigen concentrations without any dilution factors. The immunofluorocytometry bead assay kits detect lower antigen concentrations in the range of a few ng/ml with incubation times of over an hour. The microimmunoassay is intended for detecting higher concentrations in the μg/ml range, the target human systemic sample concentration range seen before and during CPB (11), with incubation times of under five minutes.

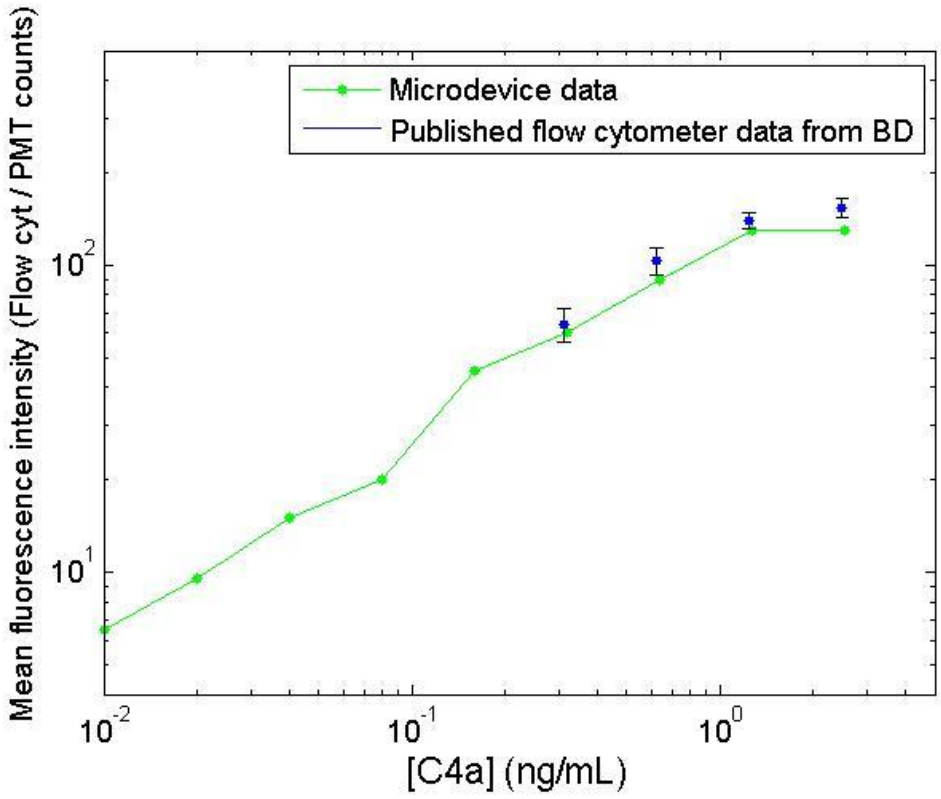

Figure 3-2: Comparison plot of commercial anaphylatoxin kit published C4a standard calibration curve with fluorescence measurements of the same beads after benchtop C4a incubation according to manufacturer's instructions followed by infusion through a microdevice with PMT fluorescence detection.

In order to validate the on-chip fluorescence detection for the dual incubation assay using the microscopy platform, the microbeads included with the commercial analphylatoxin cytometric bead assay kit were incubated with complement C4a at varying concentrations, according to the manufacturer's instructions, and analyzed within a simple microfluidic channel with the microscopy platform described below. The channel was constructed with the same technique used for the micro-immunoassay device. Data was collected and analyzed as described in section 3.5.5. The on-chip data was then compared to the published flow cytometry standards (67), as shown in Figure

3-2. Based on this comparison, it is evident that on-chip detection can yield a similar fluorescence response to that seen with a standard flow cytometer.

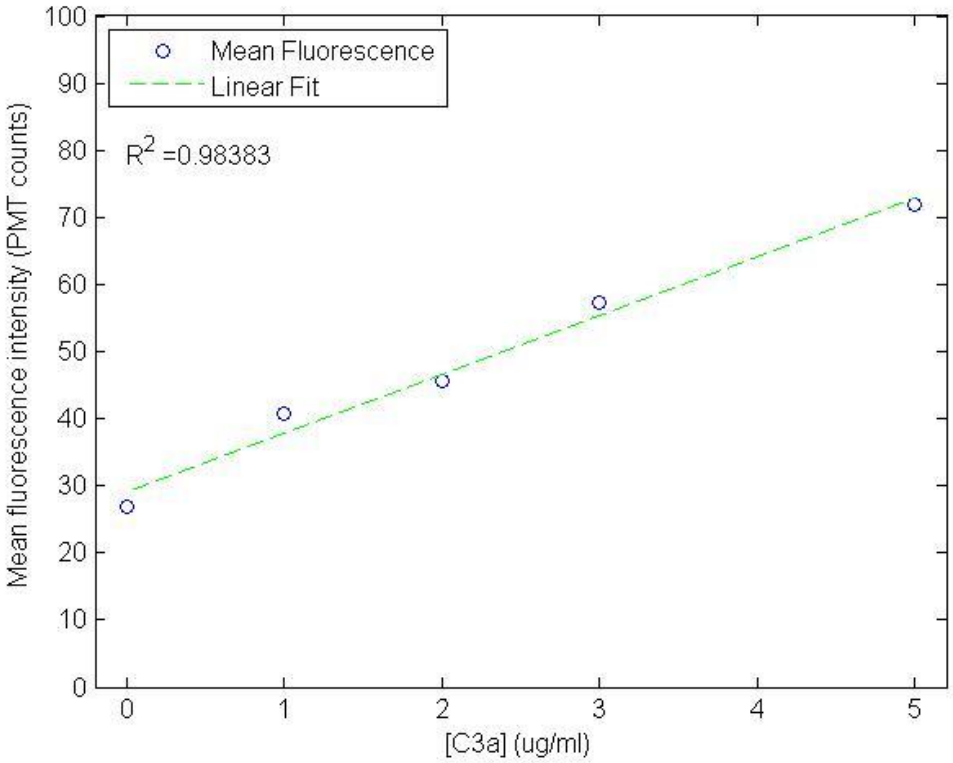

Figure 3-3: Bench-top incubated two-stage C3a antigen sandwich immunoassay fluorescence results using the paramagnetic immunofluorocytometry beads measured with a Facscaliber flow cytometer. The primary and secondary incubation times were 45 seconds each

The second bench-top experiment for the dual incubation assay tested the hypothesis of using short incubation times with higher concentrations to achieve similar total binding as long incubations with lower concentrations was tested. Since the concentrations that will be seen by the micro-immunoassay are approximately 100-1,000 times higher than those used in the bench-top kit, it was expected that a shorter incubation could result in similar fluorescence intensities. It was determined empirically that the microdevice

would be capable of incubation times of 45 seconds in each stage. Thus, a two-stage bench-top incubation was performed using the same antibody conjugated paramagnetic beads used in the micro-immunoassay, with 45 second incubations for both antigen binding and secondary labeling at concentrations in the expected systemic range (1-5 µg/ml). The beads were washed twice in PBS, then incubated for 45 seconds with the C3a antigen sample in an Eppendorf tube. The incubation was ended by adding 1 ml of PBS and vortexing. After this initial wash the beads were washed a second time in PBS, and a similar 45 second incubation with the fluorescent secondary antibody was begun. This incubation was ended in the same way as the first incubation, again washing the beads twice in PBS. Finally, the beads were resuspended in PBS and a Facsaliber flow cytometer was used to measure the mean fluorescence intensity of each sample. The results of this experiment showed that a shorter incubation time using a more concentrated analyte provides fluorescence intensities within the detection range of the flow cytometer (Figure 3-3). Based on these bench-top experiments, it was expected that the micro-immunoassay would bind a sufficient amount of analyte with its 45 second incubation times, and that the microscopy-based detection platform would be capable of measuring the fluorescence intensity of the incubated microbeads.

3.3 Microfluidic device design

3.3.1 Operating principle

The single and dual incubation microdevices both operate on the same principle: a multiple inlet channel with laminar flow patterning of reagent streams, with magnets placed along opposite sidewalls to direct the microbead trajectory, followed by fluorescence detection. The single incubation device will be described first, and the dual

incubation device will then be presented as a sequence of two single incubation channels. For the microdevice designs described, there is minimal mixing between the adjacent fluid streams since the flow is laminar at this scale. The Reynolds number for these channels with the flow rates used for experiments is approximately 5×10^{-2}, and the Peclet number is estimated to be in the range of 10^3 for biotin-FITC to 10^4 for complement C3a. All of the microdevice assays use the 8 μm paramagnetic microbeads which were tested in the bench-top assays. The first magnet pulls the beads into the antigen stream where they roll along the sidewall while incubation occurs, and the second magnet pulls them out of the sample stream across the channel into a wash stream at a precise downstream location. Figure 3-4 shows a schematic of this actuation scheme for a single incubation device.

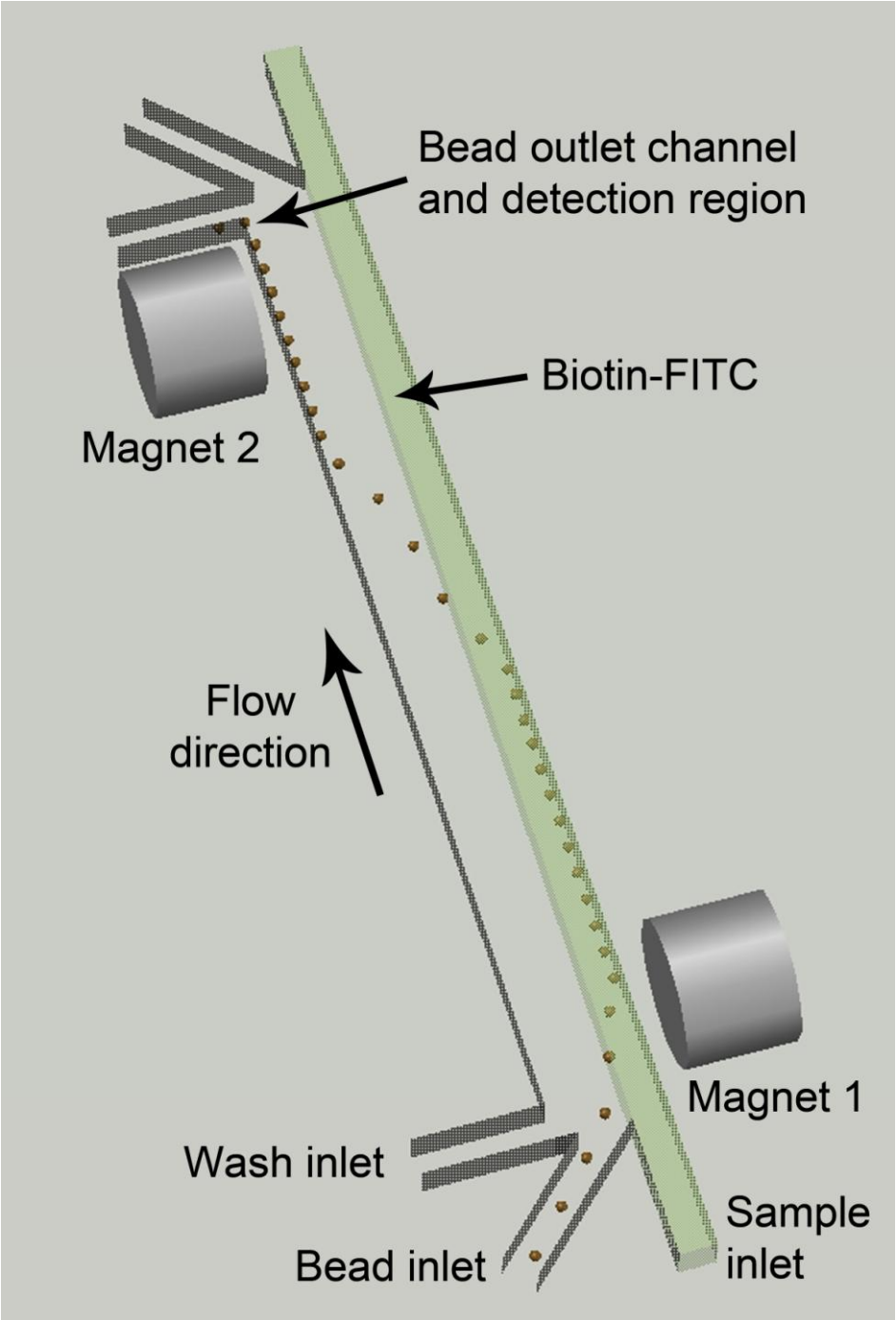

Figure 3-4: Top-view conceptual rendering of a single incubation stage magnetically actuated immunofluorocytometry microdevice. The paramagnetic beads are pulled by the first magnet into the biotin-FITC sample stream (green), and then pulled by the second magnet across the channel into the wash stream at a downstream location, followed by fluorescence detection.

The dual incubation device adds a second cycle of this scheme after the first incubation to enable a primary incubation of antibody coated beads with an untagged antigen, and a secondary incubation of the antigen-coated beads with a fluorescently tagged secondary antibody (Figure 3-5). The design allows a full sandwich immunoassay to be autonomously processed within the microdevice, relying only on the magnetic force to pull the beads to the proper sidewall, and fluid shear forces to move the bead through the microchannel. As each microbead is pulled into the final wash stream, any unbound fluorescent tag separates from the bead and is diluted in the wash fluid before the bead flows past the detection region, where optical detection occurs. Figure 3-5 shows a conceptual rendering of the dual incubation microdevice, with bead state diagrams showing the progression of binding reactions.

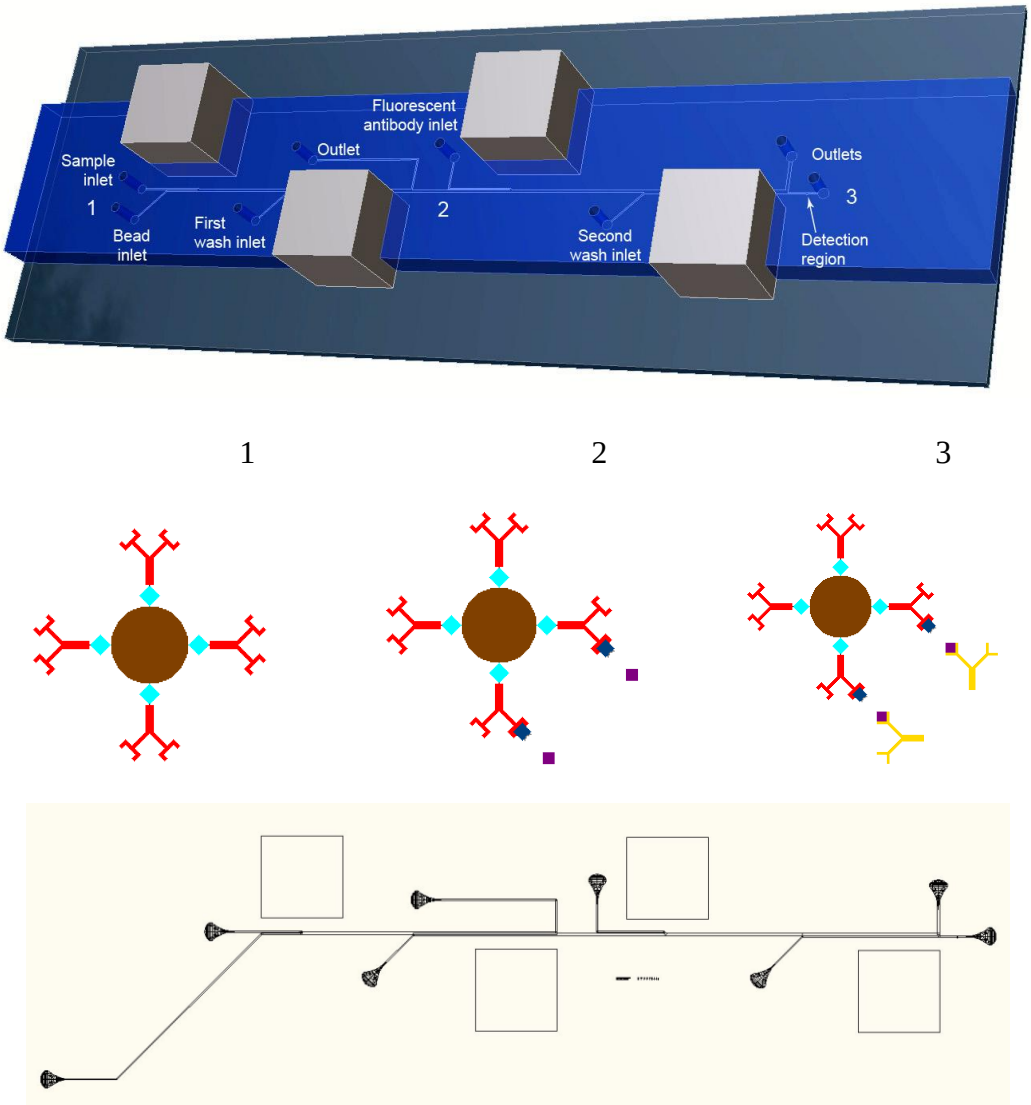

Figure 3-5: (top) Conceptual rendering from scaled 3D model of the dual incubation micro-immunoassay, with bead state diagrams at device positions 1, 2 and 3. [Position 1] The antibody coated immunofluorocytometry beads are infused into the device and pulled into the sample stream. [Position 2] After incubation the beads have antigen bound to them in an amount that is proportional to the sample antigen concentration. The beads are pulled into the first wash stream and transferred to the second stage, where they are pulled into the fluorescently labeled secondary antibody stream. [Position 3] After the second incubation all bound antigen is bound by the fluorescent tag. Finally, the beads are pulled into the second wash stream which brings them to the detection region where fluorescence intensity detection occurs. (bottom) Layout of photolithography mask for dual incubation microdevice

3.3.2 Characterization of magnetic bead actuation in a microfluidic channel

The magnetic force acting on the bead can be approximated as

$$\vec{F}_m = \frac{\frac{4}{3}\pi R_c^{\,3}\chi\vec{B}\cdot\nabla\vec{B}}{\mu_0(1+\chi)^2}$$

Equation 1

where B is the magnetic field from the magnet, μ_0 is the magnetic permeability of free space, χ is the magnetic susceptibility of the bead (χ = 0.170) (68) and R_c is the radius of the bead magnetic core (0.5 μm). Since the exact configuration of the magnetic field and gradient is complicated to model or measure on this length scale, the magnetic force on the bead is estimated to be by balancing the magnetic force with the Stokes drag force

$$\vec{F}_D = 6\pi\mu UR$$

Equation 2

where μ is the viscosity of water, U is the bead velocity towards the wall and R is the bead radius. After measuring the bead velocity to the wall to be 100 μm/sec where

$$U = \frac{\vec{F}_m}{6\pi\mu R}$$

Equation 3

the magnetic force on the bead is estimated to be approximately 7.5 pN for this system and falls off quickly as the bead rolls along the sidewall down the channel beyond the magnet face. Conversely, the fluid shear force on an 8 μm diameter bead at the channel sidewall is approximated by calculating the centerline shear stress at the bead centroid (4 μm from the wall) considering the laminar flow profile in a rectangular duct as τ = 0.111 Pa, and multiplying by the bead surface area to estimate the drag force on the bead as 22.3 pN. If the bead is off the centerline along the depth of the channel, the calculated force increases to a maximum of 28.9 pN when the centroid is 4 μm from the

top or bottom boundary. Based on these estimates, the fluid drag force is expected to be 3.0 to 3.9 times greater than the magnetic force on the beads. It should also be noted that along the face of the magnet these forces are orthogonal to each other (the magnetic force pulling the bead towards the sidewall and the shear forces propelling the beads forward) so the actual drag force on the bead as it rolls along the wall will depend on the wall dynamic frictional force (which will be a function of the orthogonal magnetic force) but is expected to be smaller in magnitude than the magnetic force. Beyond the magnet face, the magnetic force will fall off appreciably, so the shear force on the bead remains dominant as it rolls along the wall downstream of each magnet. Additionally, if the flow rate is decreased significantly (<50 nl/min) then the magnetic and shear force magnitudes approach each other and beads are more prone to being captured at the channel sidewall. In this case, the magnets need to be moved further from the channel boundaries to keep the beads from sticking. Thus, the bead incubation time of the microdevice at the flow rates used is significantly more sensitive to changes in the flow rate than it is to device-to-device variations in magnet placement.

A numerical analysis of three-dimensional streamline velocity in the microfluidic incubation channel was used to study the expected variation in bead incubation time. Based on the Navier-Stokes equation, the two-dimensional flow profile through a rectangular channel can be written as

$$u(y,z)=\frac{16a^2}{\mu\pi^3}\left(-\frac{dP}{dx}\right)\sum_{i=1,3,5\ldots}^{\infty}(-1)^{(i-1)/2}\left[1-\frac{\cosh(i\pi z/2a)}{\cosh(i\pi b/2a)}\right]\frac{\cos(i\pi y/2a)}{i^3}$$

Equation 4

Solving numerically with Matlab for a channel 200 μm wide and 20 μm deep gives the profile shown in Figure 3-6, where dark red is the highest velocity and dark blue is the

lowest. Due to the viscosity-dominant nature of this low Reynold's number flow, it can be assumed that the velocity of a microbead at any point in the two-dimensional profile will be equal to the streamline velocity at that point. Thus, it is evident that the microbead velocity across the width of the channel will be relatively constant, however the velocity from top to bottom of the channel will be more variable. The selected points in Figure 3-6 are placed at the point of maximum velocity (the channel center), and at the points along the y and z axes where the velocity has dropped by approximately 10% of the maximum. Future work may involve methods for minimizing the variation in vertical position of the microbeads to the reduce bead-to-bead variation in incubation time.

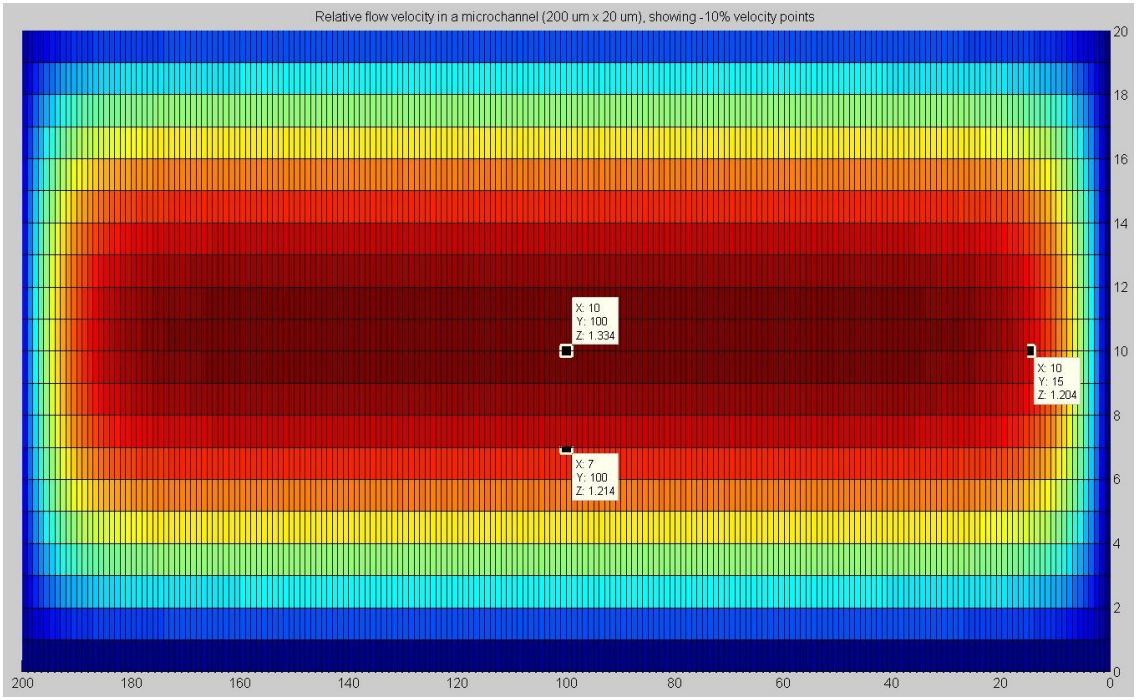

Figure 3-6: Relative flow velocity in cross sectional area of microchannel with dimensions of 20 µm in height and 200 µm in width (not to scale). The markers represent the maximum velocity point at the center of the channel, and the points along each centerline where the velocity drops by 10 percent from the maximum

3.3.3 Passive microfluidic flow control with resistance matching

When designing the dual incubation device, flow resistance matching must also be considered between the first incubation stage outlet and second incubation stage inlet. In Figure 3-5 it can be seen that the first stage outlet runs back along the length of the device further than would seem necessary. This additional channel length is included to balance the flow resistance so that two thirds of the fluid in the channel exits through the outlet, and one third continues into the second stage. The two thirds exiting represents the original bead carrier stream and the antigen stream together. Without this hydrodynamic resistance balancing, too much fluid would exit through the first outlet leaving very little flow in the second stage. The required channel length for flow balancing for the device presented was determined using a computational fluid dynamics model (Comsol Multiphysics), but it is also possible to estimate with sufficient accuracy using simplified flow resistance calculations. Figure 3-7 shows a CFD simulation of the stage transfer region, and a micrograph of a bead transferring from the first to the second incubation stage while the second magnet pulls the beads across the channel.

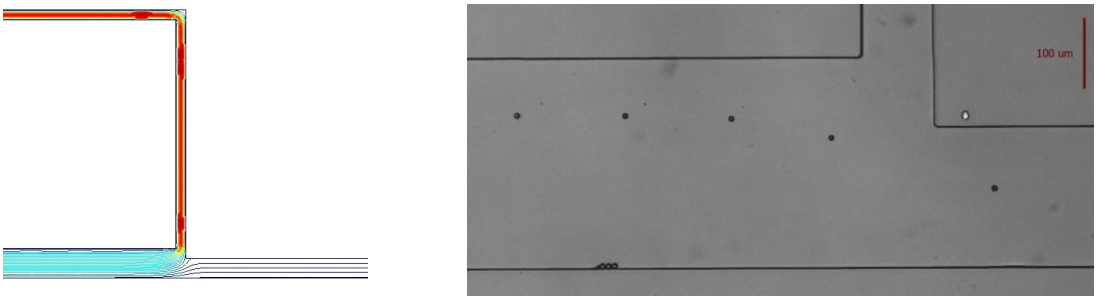

Figure 3-7: (left) CFD simulation with Comsol modeling bead transfer region between stage 1 and stage 2 of dual incubation microdevice. The color represents relative pressure with red as the highest and dark blue as the lowest. The stream lines show that by increasing the flow resistance in the waste channel a portion of the flow can be forced into the transfer channel. (right) Composite micrograph of a bead transferring from incubation stage 1 to stage 2 of the dual incubation micro-immunoassay

3.3.4 Bead injection inlet design

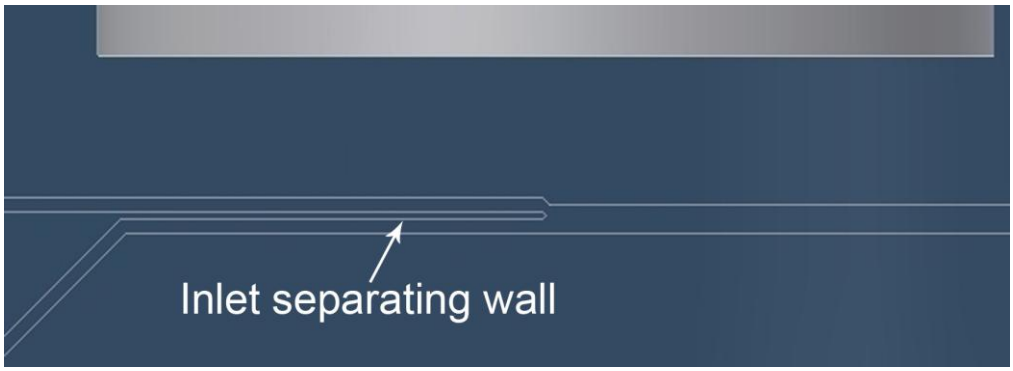

Figure 3-8: Conceptual rendering of the bead injection region. The wall between the two inlets ensures that the beads always enter the main channel from the same point

An important feature of the microchannel design is the bead injection region. In order to achieve the most consistent bead incubation possible and thus more consistent bead-to-bead response, the beads must be pulled into the sample stream at exactly the same downstream position. Figure 3-8 shows the bead injection channel design, as well as a

composite image of beads entering the sample stream. The wall between the parallel portions of the sample inlet and bead inlet allows the beads to organize against the side of the channel before being pulled into the sample stream. Previous designs that did not include this parallel region before the merging of the two channels resulted in beads scattered across the channel, entering the sample stream at significantly different locations. The special injection region design ensures that all beads enter the sample stream at the same location, therefore experiencing a consistent incubation time.

Also important to bead injection continuity is the elongated bead carrier inlet channel, visible in the lower panel of Figure 3-5. This design is required to minimize the magnetic force on the beads while they are still in the inlet tubing. While within the inlet tubing the beads must travel vertically downward into the port of the microdevice. When there is a significant magnetic field present within the tubing, the beads are pulled strongly against the wall of the tubing and remain stuck to the wall indefinitely. This problem arises mainly due to the low fluid velocity in the tubing. While the device channel sizes and the inlet flow rates are chosen to avoid bead sticking within the channels of the device, these channels have a maximum cross sectional area of 6000 square microns, while the tubing has a cross section area of over 50,000 square microns. Since the device flow rate cannot be adapted to avoid bead sticking in the tubing, the design options considered were to use smaller diameter tubing, and to reduce the magnetic field present within the tubing. While smaller diameter tubing was shown to have positive effects on reducing bead sticking in the tubing, the simplest and most robust solution was to move the inlet farther from the magnet. A minimum straight line distance from the face of the magnet to the

inlet port of 18 mm was empirically determined to eliminate bead sticking within the inlet tubing.

A uniform suspension of beads in the carrier fluid is also very important for reliable bead injection into the device. If the beads begin to settle in the syringe, tubing, or microchannel during the experiment the flow of beads will be reduced or stopped, inhibiting the assay. To mitigate this problem, the beads are suspended in Ficoll-Paque Plus, which has a density of 1.077 g/ml. This density is similar to the microbeads' mean density of 1.07 g/ml, providing a uniform suspension for many hours.

3.3.5 Bead detection outlet design

The outlet channel containing the detection region is also designed for accurate control of microbead trajectories, in this case to reduce bead aggregation. Bead aggregates in the detection region artificially increase the effective bead fluorescence intensity seen by the detector, and therefore must be avoided. These aggregates are separated when the beads experience a large increase in flow velocity, which can be easily accomplished by reducing the relative channel width. The design presented uses a doubling of the flow velocity as the beads enter the bead outlet channel to separate aggregated beads. The flow velocity is subsequently reduced once again when the channel widens briefly for fluorescence detection, however the beads do not aggregate in this brief time.

3.3.6 Microdevice fabrication

The microdevices were fabricated by standard soft lithography (69, 70) using an SU-8 master mold with a feature depth of 20 μm. The PDMS was cast to a thickness of 4 to

5 mm so that the PDMS could mechanically support external magnets placed at the periphery of the microchannels. The device inlet and outlet ports were punched with a sharpened 19 gauge needle. The PDMS was then bonded to a standard 75 mm × 25 mm glass slide. Bonding was accomplished by treating the PMDS and glass with a corona discharge (Electro-Technic Products, Inc., Chicago, IL. BD-10AS) for approximately 10 seconds, pressing the PDMS to the glass, and placing the device in a 100 °C oven for 2 hours. The slots for the magnets were cut by hand with a razor blade. Neodymium magnets with a 5,754 Gauss surface field, measuring ¼ inch on each side, (K&J Magnetics, Jamison, PA, No. B444) were pressed into those slots so that their magnetic fields were all aligned in the same direction across the width of the microchannels. The magnet faces were approximately 3 mm from the edge of the incubation microchannel. The main channel width for all microdevices was 300 µm with 100 µm wide inlet and outlet branches. Both devices had incubation channel lengths of approximately 1 cm (point from bead entering incubation flow to entering wash flow).

3.4 Microdevice assay detection platform

The microdevices experiments utilized an epifluorescence microscopy platform with a Nikon TE2000U inverted microscope at 30× magnification. The devices were loaded into a device holder on the microscope, and a 30 mW, 488µnm beam emission from an argon ion laser (Modu-Laser, Stellar-Pro-CE) was focused through the microscope to the detection region of the microdevice. The 30× magnification results in an approximately 20 µm spot size for the focused beam. A photomultiplier tube (PMT) (C&L Instruments, Hershey, PA Model DPC-BA) was mounted to the side camera port of the microscope to measure the emitted light intensity at 200 samples per second. A filter block with a

480 nm bandpass excitation filter and a 488 nm dichroic mirror was used for excitation. For experiments with fluorescein (FITC) as a fluorescent tag (used during single incubation experiments), a 535 nm bandpass emission filter was used. For experiments with Phycoerythrin (PE) (used during dual incubation experiments) the emission filter was replaced with a 580 nm bandpass filter.

3.5 Microdevice assay experimental procedure for discrete samples

The fluids used during all experiments were loaded into 1 ml plastic syringes. The syringes were placed in syringe pumps (PicoPlus 22, Harvard Apparatus), and 0.01 inch ID Tygon Micro Bore PVC tubing (SmallParts Inc., Miramar, FL) was run from each 30 gauge syringe needle to the associated inlet ports (shown in Figures 1 and 2). The tubing was pressed into each pre-punched port using tweezers with no further sealing necessary. Similarly, tubing was run from each outlet to a glass beaker for waste collection. The syringe pump containing the wash fluid syringe was first turned on and run at 3 µl/min. This flow helps to purge air from the device, and a small amount of bovine serum albumin (BSA) in the wash solution helps to reduce bead sticking in the channel when it is precoated. The remaining syringe pumps were then turned on and run at 3 µl/min to continue purging air from the device. They were then set to the desired infusion flow rate for the experiment, and after a brief settling time the concurrent flows stabilized and measurement began. After running each discrete sample concentration, the sample syringe was removed and replaced with the next sample, the device was again purged, and measurement of the new sample commenced.

3.5.1 Single incubation microdevice experimental setup

The streptavidin coated paramagnetic beads were first washed twice with phosphate buffered saline (PBS) (25 µl of bead stock in 1 ml of PBS). The beads were then resuspended in 500 µl of Ficoll-Paque Plus (GE Healthcare) for a better density match between the beads and carrier fluid. The final bead density was approximately 1.6 million beads per ml. The analyte for the single incubation assay was prepared by serial dilution of biotin-FITC in PBS. The biotin-FITC concentration ranged from 0.025 to 0.75 µg/ml. The three fluids prepared for the single incubation assay included the streptavidin-coated bead carrier solution, the biotin-FITC sample solution, and PBS with 0.01% BSA for the wash stream. The single incubation device experiments used a flow rate of 300 nl/min at each inlet.

3.5.2 Single incubation proof of concept microdevice experimental results

Complete on-chip incubation and detection experiments were conducted using the single incubation microdevice at a flow rate of 300 nl/min from each syringe for the bead carrier fluid, biotin-FITC sample, and PBS wash solution. Figure 3-9 shows a conceptual rendering of the single incubation, straight channel device, along with a composite micrograph showing the trajectory of beads being pulled by the first magnet into the sample stream.

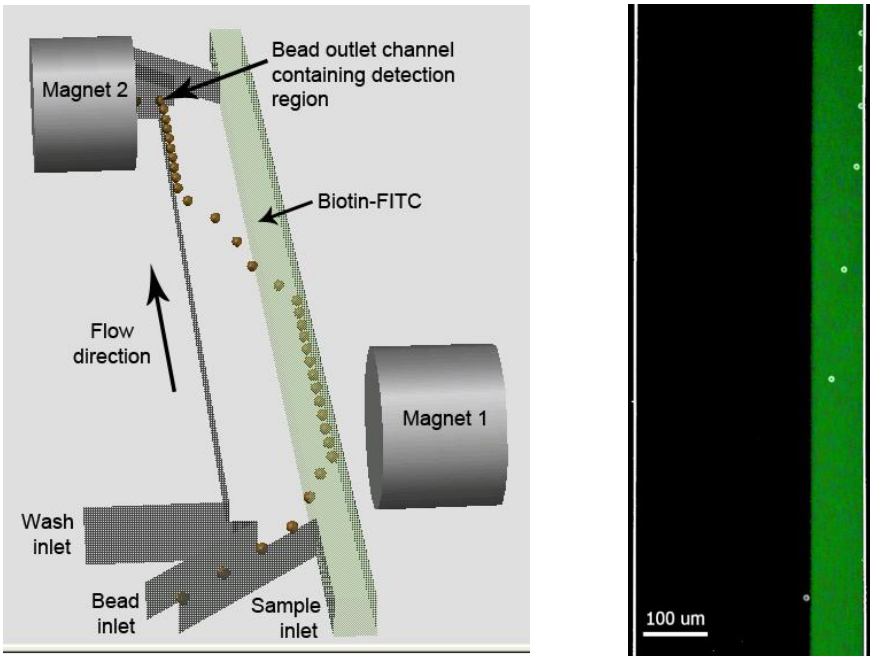

Figure 3-9: (left) Conceptual rendering of single incubation, straight channel device. (right) Composite micrograph of beads being pulled into biotin-FITC sample stream by first magnet. A bright-field image of beads flowing into the channel is overlaid with an epifluorescent image of the same channel with the biotin-FITC sample stream fluorescing in green

The results for the single incubation microdevice assay are shown in Figure 3-10. The bead incubation time in the biotin-FITC stream in the microdevice was 18 seconds at this flow rate. Approximately 300 bead fluorescence events per minute were recorded for this assay. Results from this assay show a linear fluorescence versus concentration response provided that the incubation remains in the linear portion of the streptavidin-biotin binding curve.

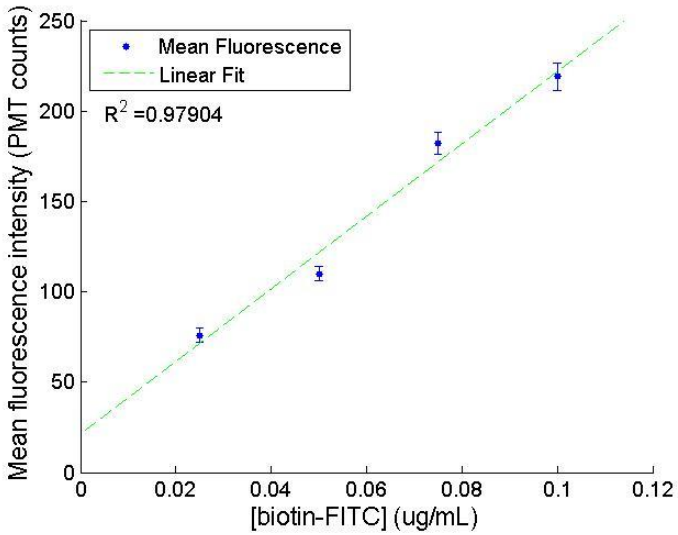

Figure 3-10: Bead fluorescence versus biotin-FITC concentration from on-chip incubation and detection using a single incubation stage device

3.5.3 Dual incubation microdevice experimental setup

For the dual incubaiton assay, 25 µl of the streptavidin coated paramagnetic beads were washed twice with PBS and then resuspended in 50 µl of PBS. They were then incubated with 5 µl of a 1 mg/ml biotinylated primary monoclonal anti-human C3a antibody stock (Assay Designs Ann Arbor, MI, catalog number GAU017-01B) at room temperature for 1 hour in an Eppendorf tube. An excess of antibody was used to ensure complete antibody conjugation to the beads. The beads were then washed again twice in PBS, and resuspended in 500 µl of Ficoll-Paque Plus. The complement C3a samples used in the dual incubation assay were prepared by serial dilution of a stock solution (EMD Chemicals, Gibbstown, NJ) with PBS. The C3a concentration used ranged from 0 to 5 µg/ml. The fluorescently labeled secondary antibody (anti-human C3a antibody) for the dual incubation assay (Assay Designs Ann Arbor, MI, catalog number GAU013-16) was

prepared using a phycoerythrin (PE) fluorescent dye conjugation kit according to the manufacturer's instructions (Prozyme, Inc., San Leandro, CA). After resuspending 50 µg of the fluorescently tagged antibody (assuming 100% recovery after labeling) in 1 ml of PBS, the labeling antibody solution was diluted with PBS to a final concentration of 12.5 µg/ml for use in the microdevice. The five fluids prepared for the dual incubation micro-immunoassay included two wash streams (PBS with 0.01% BSA), the antibody coated bead stream, the C3a antigen solution, and the fluorescently labeled secondary antibody solution. The dual incubation assay used a flow rate of 100 nl/min at each inlet, resulting in an empirically determined 45 second incubation time per stage.

3.5.4 Dual incubation micro-immunoassay experimental results

Complete on-chip incubation and detection experiments were conducted using the dual incubation microdevice at a flow rate of 100 nl/min from each syringe for the bead carrier fluid, C3a sample, fluorescent secondary antibody stream, and two PBS wash streams. A photograph of a complete dual incubation, straight channel microdevice is shown in Figure 3-11 (Conceptual rendering is shown in Figure 3-5 in section 3.3.1). The data are shown in Figure 3-12. The device was able to distinguish between samples with different concentrations of complement C3a in the expected clinical range of 1 to 5 µg/ml. The data are discussed in further detail below.

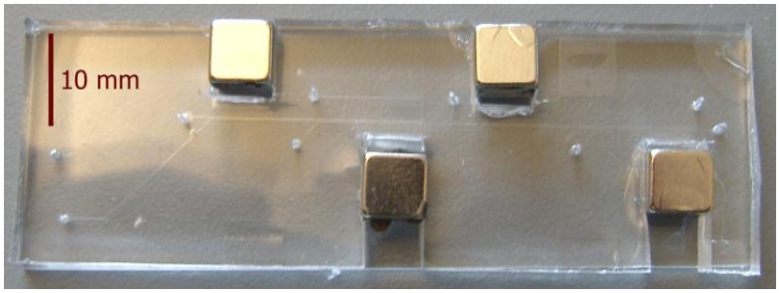

Figure 3-11: Photograph of complete dual incubation, straight channel microdevice

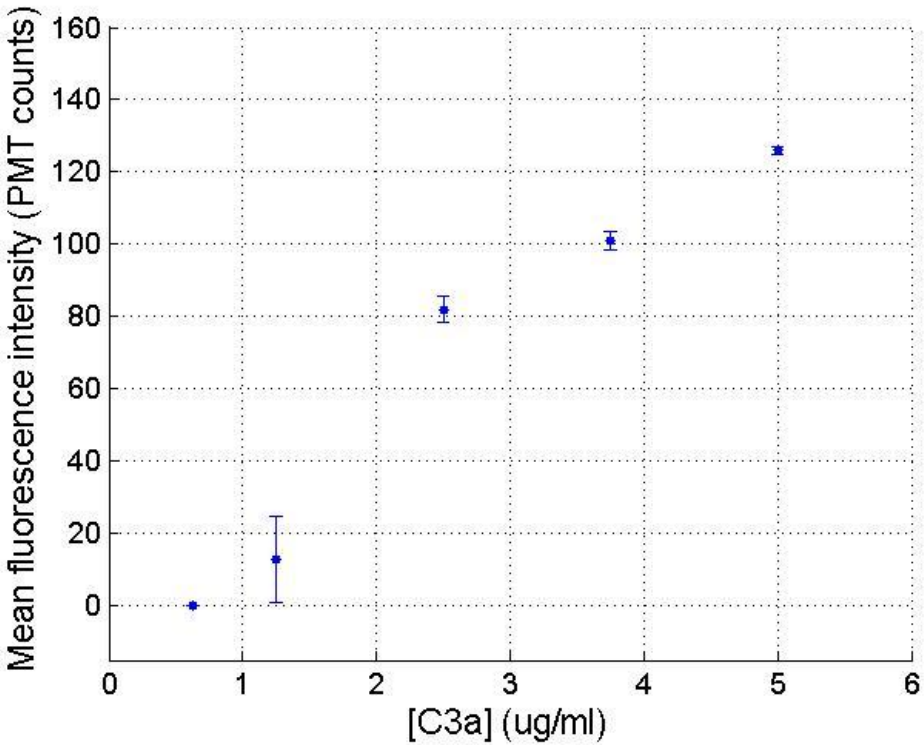

Figure 3-12: Results from the dual incubation micro-immunoassay with fully autonomous on-chip incubation and detection, showing fluorescence intensity in PMT counts versus C3a antigen concentration. The error bars show the standard error about the mean

3.5.5 Data collection and processing for discrete samples

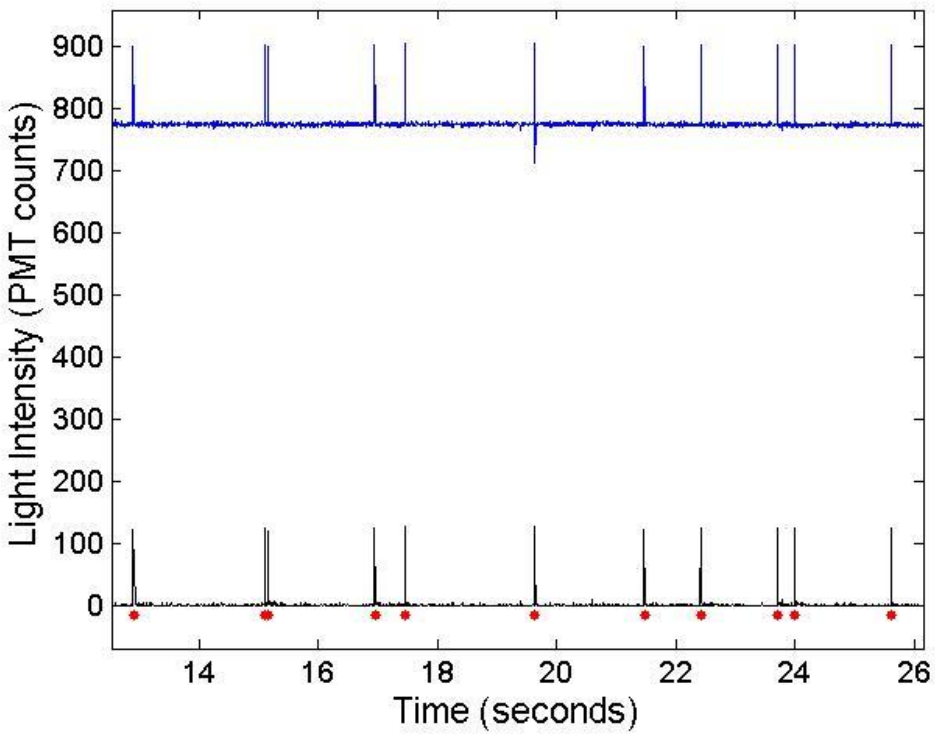

Figure 3-13: Partial PMT trace from the dual incubation experiment showing the original detected signal (top) and signal after high-pass filtering (bottom). The dots represent each peak detected by the peak finding algorithm

The bead fluorescence intensity is recorded by monitoring the PMT output as the beads pass through the focused laser light within the device detection region. A PMT sampling rate of 200 Hz was empirically determined to be sufficient for the flow rates used during the experiments. The sampling rate must be sufficiently fast as to capture light from any passing bead while it is near the center of the field of view of the detection region. If the sampling rate is too low relative to the velocity of the beads in the detection region, multiple beads may pass the detector during the sampling time. As the sampling

rate increases, the amount of light captured in each sample is lower, reducing the signal to noise ratio. Each fluorescence sample represents a count of photons within a 5 ms time period. The fluorescence intensity data collected by the PMT was then processed with a 1 Hz Butterworth high-pass filter and a custom peak finding algorithm written with Matlab. The filter shifts the PMT intensity baseline to zero and removes any baseline fluorescence drift. After filtering, peaks with a trailing edge drop-off greater than two standard deviations of the dataset mean were counted as bead fluorescence events. The peak values were then averaged to find the mean bead fluorescence intensity for the sample.

Figure 3-13 shows a representative PMT trace using a 5 μg/ml C3a sample before and after filtering. The Butterworth filter shifts the PMT intensity baseline to zero and removes baseline drift before the data is processed by a peak finding algorithm. The high-pass filter together with the peak finding algorithm remove the background fluorescence from the bead fluorescence measurements. Peaks with a trailing edge drop-off greater than two standard deviations of the dataset mean are counted as bead fluorescence events. These are shown by the dots in Figure 3-13. The measured fluorescence intensity for each tested sample is determined by finding the mean value of the peak maxima. Fluorescence histograms of three datasets after filtering are shown in Figure 3-14. For samples with moderate to high antigen concentrations, the dataset histograms show a Gaussian distribution around the mean bead fluorescence value, and low values of standard error. This distribution is similar to that of a traditional bench-top incubated immunofluorocytometry assay using a standard flow cytometer for detection as shown in Figure 3-15. At concentrations closer to the lower limit of the device's detection range,

the bead intensity histogram peak has a lower signal to noise ratio and begins to merge with the baseline noise. At this point a Gaussian peak is no longer discernable and the standard error increases. At even lower concentrations, the mean peak value is equal to that of the system noise alone, which was around 12 counts, or 1% of the 10-bit measurement range of the PMT, for the experimental parameters used. For the device parameters used here, the dual incubation microdevice assay was unable to differentiate a sample at a C3a concentration of 625 ng/ml from background noise, and if sample concentrations below this were to be processed a longer incubation channel and/or lower flow rate would be used to increase the incubation times and achieve a sufficient bead fluorescence signal.

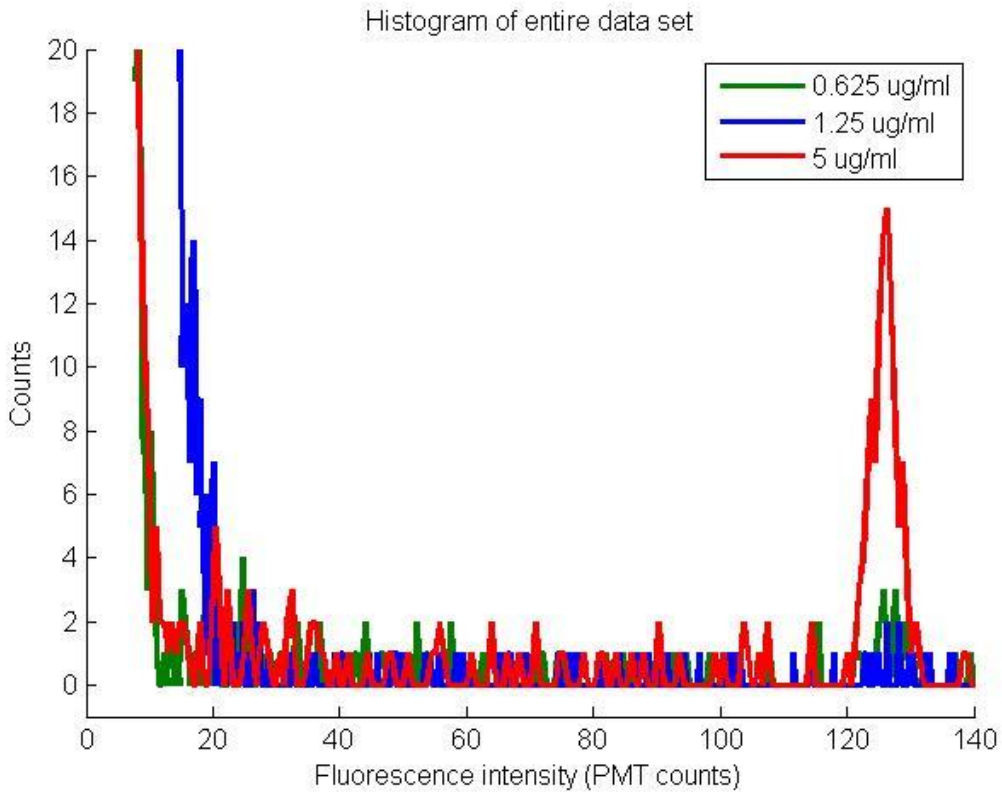

Figure 3-14: Overlayed fluorescence intensity histograms of three datasets from the dual incubation micro-immunoassay experiments, using C3a sample concentrations of 5 μg/ml, 1.25 μg/ml, and 0.625 μg/ml. At the lowest concentration, the intensity histogram merges completely with the baseline noise, thus representing the detection limit of the assay

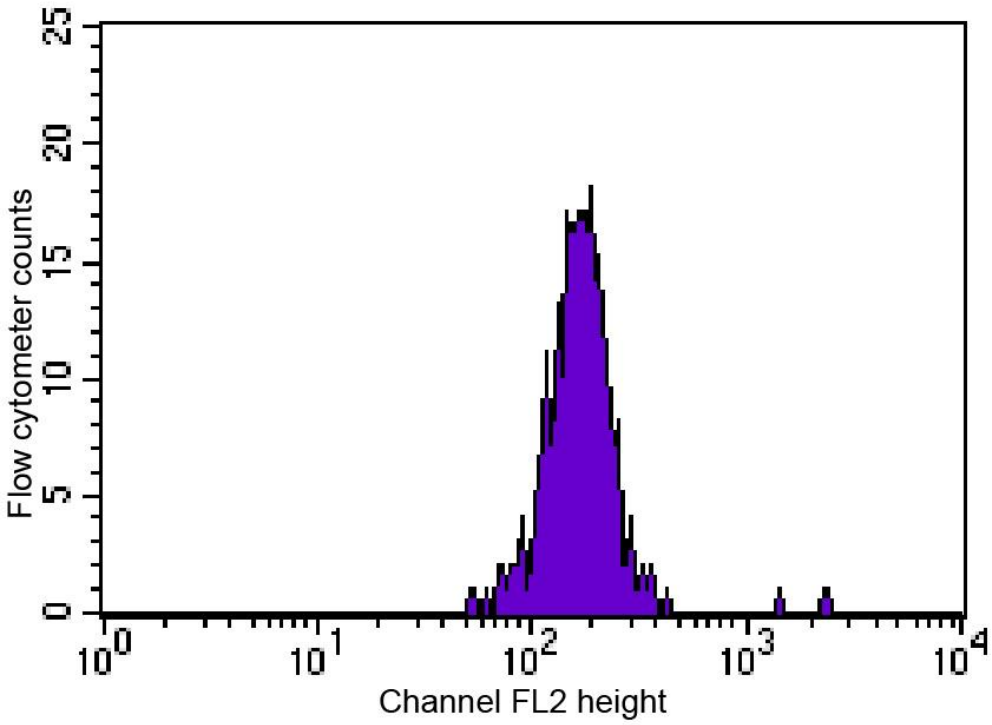

Figure 3-15: Representative histogram from flow cytometer for a 5 μg/ml C3a sample with a 2 minute bench-top incubation. An ideal dataset is expected to show a Gaussian distribution around the mean fluorescence intensity

4 EXTENDED INCUBATION CHANNEL DEVICE

4.1 Overview

The dual stage micro-immunoassay device was subsequently modified to provide a longer incubation channel, leading to longer incubation times at higher flow rates. Longer incubation times increase the sensitivity of the assay at low analyte concentrations. Higher flow rates make the bead manipulation more reliable since shear is increased overall, reducing the tendency of microbeads to stick to the channel walls. The increased incubation channel length was provided by diverting the sample stream, subsequent to the bead crossover point, into a long spiral channel. A conceptual rendering of the modified design is shown in Figure 4-1, as well as a channel layout. Each incubation channel is approximately 30 cm in length, which is 30 times longer than the straight incubation channel.

The spiral incubation channel design also provides additional benefits. Since the microbead trajectory is reversed subsequent to the spiral region, the beads pass the center of the device two times on each layer. This allows a single magnet to be used for all magnetic actuations. This design also allows the beads to transfer directly from the antigen stream to the secondary antibody stream, eliminating the need for the first wash stream, and reducing the number of inlet streams from 5 to 4.

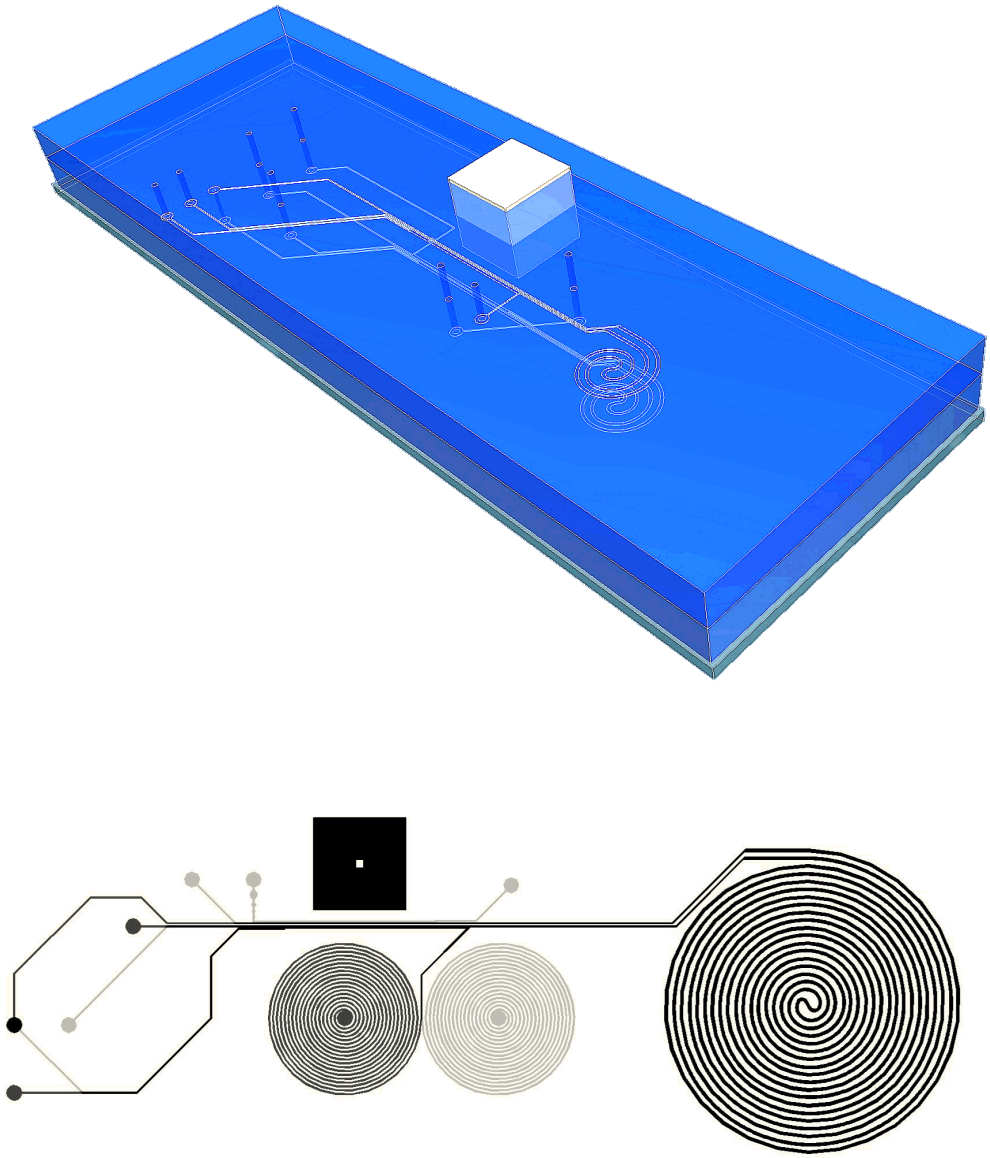

Figure 4-1: (top) Conceptual rendering of dual incubation micro-immunoassay device with spiral design extended incubation channels. (bottom) Layout of the device showing top layer in dark gray and bottom layer in light gray. The large spiral is identical in both layers.

4.2 Single incubation spiral device experimental results for discrete samples

The spiral incubation channel device, shown conceptually in Figure 4-1 (dual incubation version), lends itself to reliable control of incubation times by varying the flow rate. The single incubation device was validated by running three different flow rates at a constant biotin-FITC concentration of 10 ng/ml (15 nM). The results showed a linear relationship between mean fluorescence intensity and incubation time (Figure 4-2). It is also evident that the assay sensitivity is improved over the shorter incubation channel device (Figure 3-10).

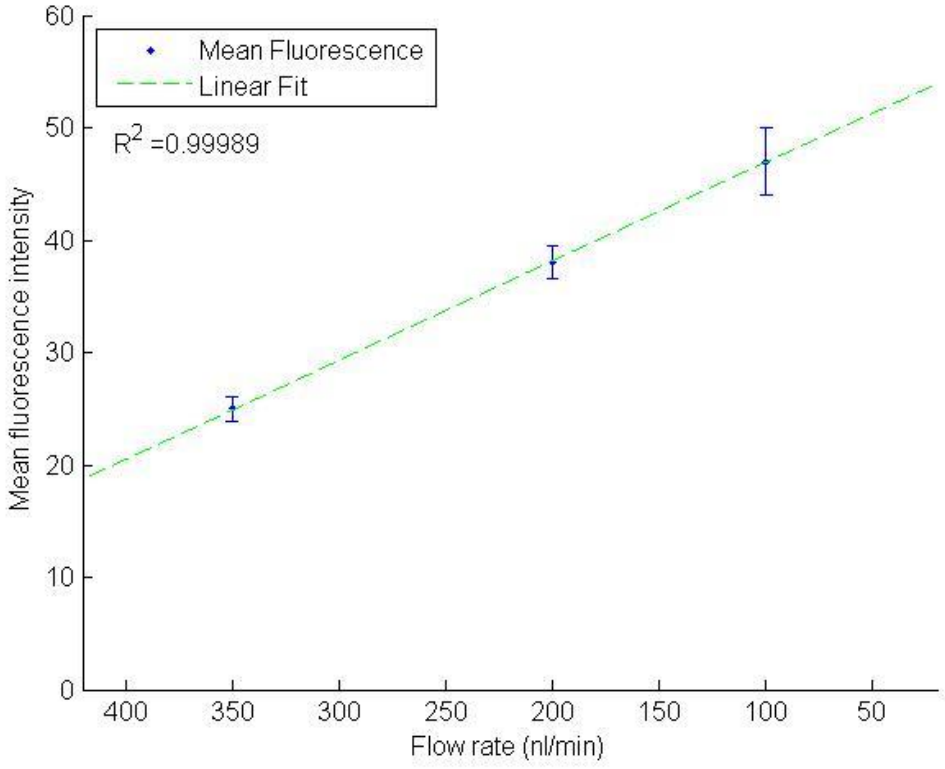

Figure 4-2: Varying incubation time by changing flow rate with single incubation device with 15 nm biotin-FITC sample. The approximate incubation times for each flow rate are 4, 7 and 14 minutes

4.3 Dual incubation spiral device calibration and benchmarking

Experiments with the dual incubation, spiral channel device were performed at a flow rate of 1 μl/min at all inlets. The incubation time for each stage was approximately 2.5 minutes. The results were similar to those from the dual incubation straight channel device, but the fluorescence intensities were higher for a given concentration due to the increased incubation time. While device fabrication in notably more complicated for the spiral device as compared to the single layer straight channel device, the spiral channel device was more robust and reliable during operation. The calibration curve for the spiral channel experiments is shown in Figure 4-3.

A similar calibration curve (Figure 4-5) was used to generate the data in Figure 4-4. The pair-wise scatter plot compares measurements of C3a concentration from stored blood samples using the novel microfluidic assay and a commercial ELISA kit. The calibration standards were also assayed using the ELISA kit to ensure that standards and blood samples with the same C3a concentration give the same result in the novel assay.

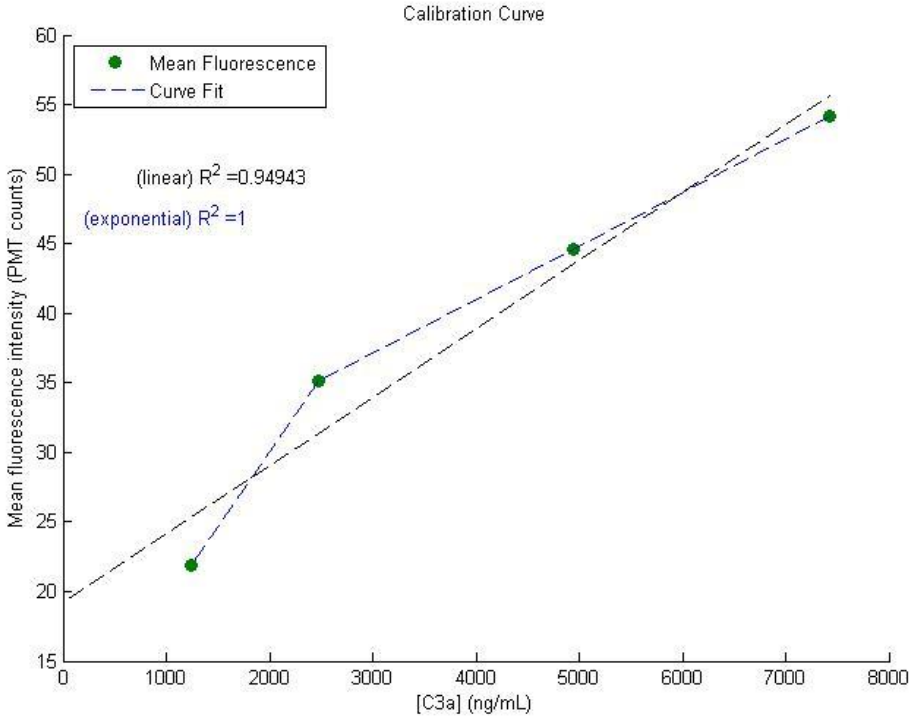

Figure 4-3: Results from dual incubation spiral device with discrete samples of complement C3a, showing linear and exponential curve fit. The nonlinear response at lower concentrations is typical for this assay

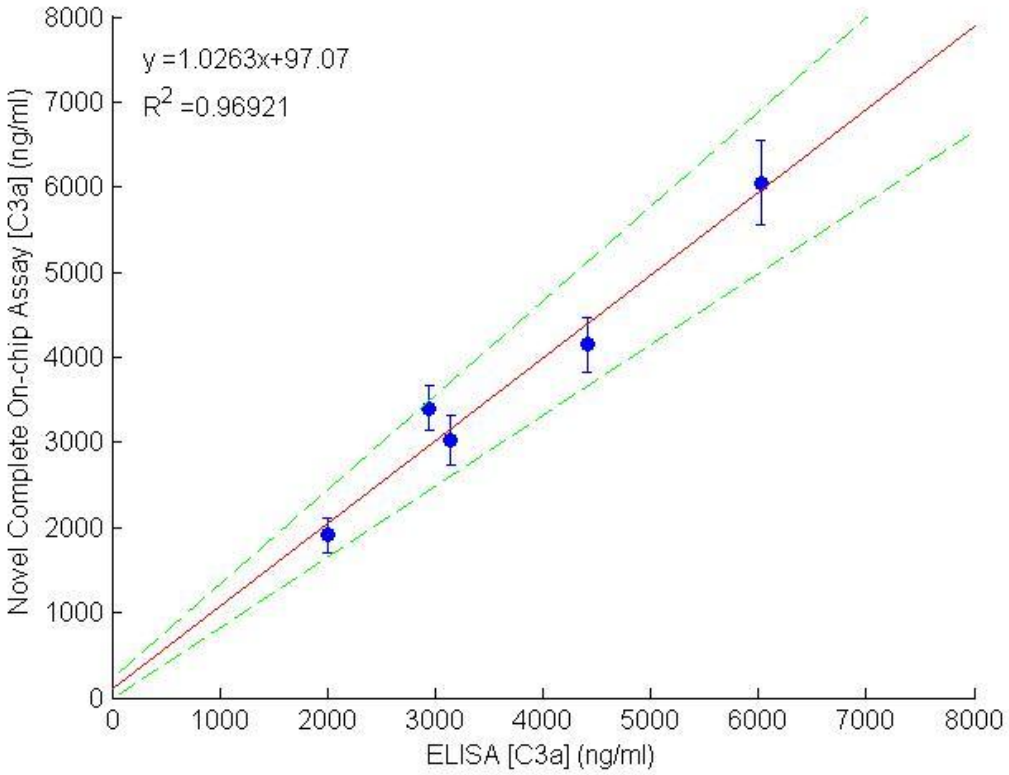

Figure 4-4: Pair-wise scatter plot comparing C3a concentration measurements made on collected blood plasma by the micro-immunoassay device with those made using a standard ELISA plate

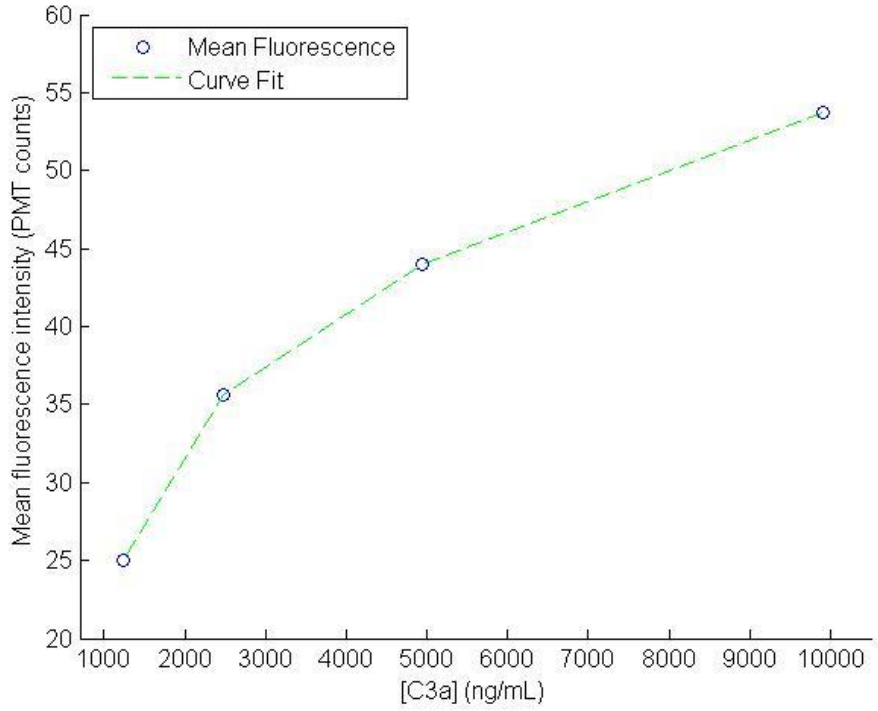

Figure 4-5: Calibration curve for micro-immunoassay used for benchmarking against ELISA. The calibration is based on serially diluted C3a standards

4.4 Temporal response experiments with inlet mixer

4.4.1 Temporal response experimental procedure

Temporal response experiments were conducted using a single incubation version of the extended incubation device. These experiments are intended to ascertain the transient response characteristics and repeatability of the system. To enable a time-varying sample concentration, a mixer channel was added to the sample inlet channel on the microdevice. The mixer is simply a long zigzag channel with sufficient length to allow diffusional mixing of two streams. The sample stream was composed of a stream with a known concentration of biotin-FITC, and a PBS dilution stream. The relative flow rates were

varied to control the concentration after the mixer, while the total flow was held constant. Each stream was sourced from a separate, remotely-controllable syringe pump (PicoPlus 22, Harvard Apparatus). The pumps were controlled by a custom Visual Basic program. The program adjusted the flow rates of the two pumps every 30 seconds following a sinusoidal concentration curve with a defined period and amplitude. The remainder of the experimental setup was identical to the steady-state experiment described in section 3.5, "Microdevice assay experimental procedure for discrete samples".

4.4.2 Data collection and processing for temporal response

Data from temporal response experiments was collected and recorded in the same way as described in section 3.5.5, "Data collection and processing for discrete samples", by detecting and recording the position and magnitude of PMT output peaks. The peak data was then processed by an algorithm which performed filtering and statistical analysis, which was written with Matlab. A finite impulse response (FIR) filter was performed by windowing overlapping 60 second subsets of the data set, and finding the mean peak value in each window. The algorithm counted approximately 300 beads events (peaks) in each 60 second window. This algorithm allows for the window width to be adjusted, where smaller windows result in greater detail and larger ones in reduced noise.

4.4.2.1 Temporal response characterization results with single incubation spiral device

Data from the temporal response experiments are shown in Figure 4-6. The plot on the left shows a step-wise increase in concentration, which could be used for calibration. The right side shows a high frequency, high amplitude sinusoidal change in frequency.

The results seem to suggest that the assay is repeatable in the steady state, but unable to track very high rates of change. Further research would be necessary to determine the maximum rate of change in the biological systems being assayed.

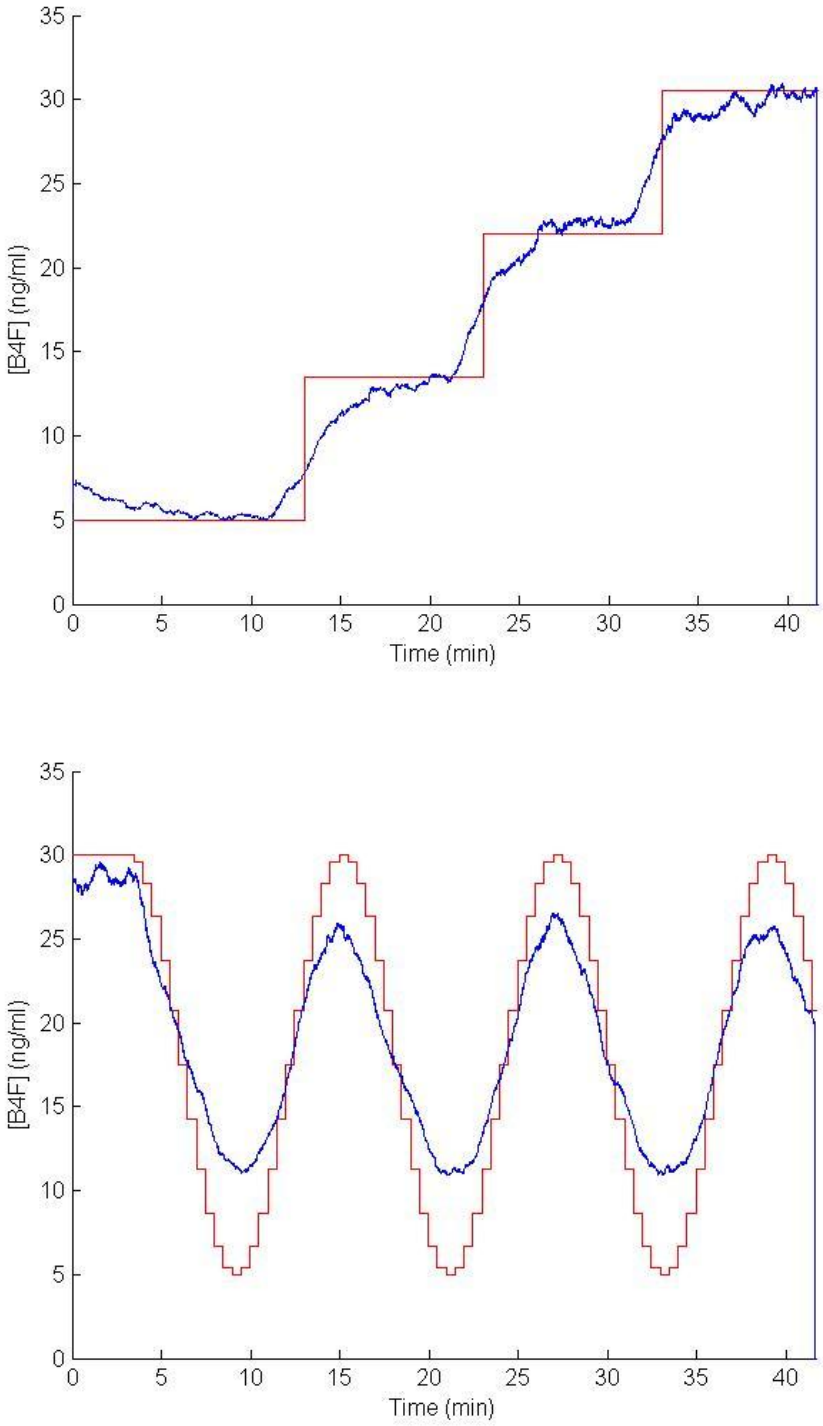

Figure 4-6: Temporal response using single incubation spiral device. (left) Step response; (right) Response to a high frequency sinusoidal input. The red lines show the theoretic concentration, while the blue lines show the measured concentration. High rates of change of concentration exceed the maximum temporal response of the device

4.5 Continuous monitoring proof of concept

4.5.1 Overview of requirements

In order to apply the microfluidic immunosensor to monitoring of a native sample stream, additional system development is required. In the previous sections, the sample fluid was always loaded into a syringe and infused into the device using a syringe pump. The microfluidic device design relies on matched source flow rates for proper functioning, which is easily controlled when all sources are infused by flow rate controlled syringe pumps. For Specific Aim II, a syringe pumping scheme is no longer applicable for the sample fluid. A system must be designed which allows continuous sample pumping from a source reservoir with infusion at a constant flow rate. Furthermore, the presence of cells in the blood which are similar in size to the microbeads used in the assay requires the addition of an inline sample filter. The microfluidic device used in all continuous monitoring experiments is the dual incubation device with spiral incubation channels described in section 4.

4.5.2 Continuous sample infusion system with peristaltic pump

The sample infusion system for infusion of native sample streams is based on a small peristaltic pump (Instech Laboratories model P720, Plymouth Meeting, PA). This type of pump was chosen due to its availability, robustness and the high pressure head which it can develop. Certain characteristics of this type of pump must be considered in this application. Unlike a syringe pump, the peristaltic pump has imprecise flow control, and its flow rate varies with the flow resistance into which it is pumping. Furthermore, the head pressure is not continuous, but rather it is a periodic variation similar to an

alternating current signal superimposed on a direct current signal. The periodicity occurs due to the three-roller design of the pump. Each of the three rollers must disengage from the tubing once per revolution, and at this point the head pressure quickly but momentarily drops below the required inlet pressure. Since the operation of the microfluidic device relies on a precise and steady sample flow, the pump must be complemented with a flow modification system involving both electronic and mechanical components.

4.5.2.1 System components

Three components are added to the sample infusion system to modify the sample flow. The components are connected to the sample inlet channel of the microdevice downstream of the pump inlet. Thus, the unmodified output of the peristaltic pump reaches the inlet channel of the device, and the flow is modified within the sample inlet channel of the microfluidic chip. The components connected to the channel downstream of the pump input, listed in order, are a solenoid-actuated valve, an air reservoir damper, and a pressure sensor.

The valve (BioChem Valve, Boonton, NJ), and the pressure sensor (Honeywell Sensing and Control, ASDX030G24R) act together to create an active pressure control system. Since the remaining inlet streams are infused at highly controlled flow rates by syringe pumps, the sample flow rate can be maintained by controlling the inlet pressure to a predetermined setpoint. This setpoint can be determined by running the device with syringe pump infusion on all inlets (including the sample inlet) and measuring the pressure generated at the inlet channel. A microcontroller circuit, detailed below, is used to monitor the pressure and actuate the valve as necessary. The valve is able to bleed off

excess flow to reduce the inlet pressure to the set point. The valve can reduce pressure when the pump is providing excess flow, which is the case for the majority of time. The valve cannot, however, increase the inlet pressure above the pump's head pressure for instances when the head pressure drops. The damper is added to smooth pressure drops caused by roller disengagement. These events allow the pump head pressure to drop below the required inlet pressure for a brief period. The damper is simply a 3 ml plastic syringe. The plunger of the syringe is retracted, filling it entirely with air before connecting it to the microdevice. When the system is running, the pressure in the syringe builds up so that it is equal to the inlet pressure. When the inlet pressure drops momentarily, the air column in the syringe acts like a spring pushing fluid into the device and maintaining the inlet pressure.

A final component of the continuous blood sampling system is an inline filter to remove cells from the sample stream before they enter the device. A microfiltration device is used which is based on the design described in Aran et al. (71). In this designn, a membrane is bonded between two layers of PDMS which are patterned with channels. One side of the membrane is the reservoir side and the other is the filtrate side. The reservoir side has a blood inlet and an outlet for excess flow, while the filtrate side has only an outlet for the filtered blood plasma. The device is connected to the system using the same type of tubing connections that are used for the micro-immunassay device detailed in section 3.3.6, "Microdevice fabrication". To avoid application of high pressure to the filtration device, the peristaltic pump is located downstream of the filter.

4.5.2.2 Controller design

The active pressure control circuit is based on reprogrammable microcontroller with an integrated analog to digital converter and pulse modulation output (Microchip Technology, Chandler, AZ). The microcontroller is programmed to sample the output of the pressure sensor at least 1000 times per second, and calculate the difference between the current pressure and the setpoint. This value is used in the control algorithm to determine the valve output. The pulse modulation output of the chip is used to control the valve position, with a field effect transistor sinking current from the solenoid. Using pulse width modulation, the controller output can vary the valve position from 0 to 100 percent open in finely controlled increments.

4.5.2.3 Pressure control algorithm

The pressure control system is analogous to an electrical rectifier/regulator circuit. In this analogy, the input signal would be a DC voltage overlaid with an AC voltage. In this system, when the desired output voltage is below the DC bias, a rectifier diode can be used to clamp the voltage down. The rectifier handles any condition where the input voltage is greater than the desired output. On the other hand, if the AC component of the signal causes the input voltage to drop below the desired output voltage, a capacitor is applied to smooth the output voltage by supplementing the output with stored charge. As long as the mean signal voltage is greater than the desired output voltage, it is possible to smooth voltage troughs with a large enough capacitor. The rectifier diode is analogous to the actively controlled bleed-off valve in the pressure control circuit. In this case the setpoint can be adjusted on-the-fly through computer software which communicates with the microcontroller. Also adjustable is the duty cycle applied to the valve in the open

position. A greater duty cycle results in a lower resistance to flow. This setting is analogous to a resistor which is placed in series with a rectifier diode. If the flow is too fast, the pressure will be bled off too quickly and will not be controllable. If the flow is too slow, the pressure will not bleed off quickly enough to lower the head pressure applied by the pump. The damper component is analogous to the capacitor. A very large damper can smooth large troughs in head pressure, but it takes more time to build the initial pressure in the damper. This time can be circumvented by installing a valve in the tubing which feeds the damper so that a second syringe can be used to prime damper.

The microcontroller constantly monitors the system pressure and opens or closes the valve as necessary. The valve open duty cycle is adjusted by trial and error to achieve steady pressure control. The software allows the pressure to be recorded and subsequently plotted to analyze the quality of control throughout the assay. The target peak-to-peak pressure fluctuation is 1% or less. There is an overpressure safety point at 1 psi above the control setpoint which opens the valve fully to avoid over-pressurizing the microfluidic device if the valve open duty cycle is set too low.

4.5.3 Experimental procedure for continuous monitoring

For all aspects other than sample infusion, the setup of the microfluidic device for integration with the CPB circuit is identical to that described in sections 3.5, “Microdevice assay experimental procedure for discrete samples”, and 3.5.3, “Dual incubation microdevice experimental ”. The bead carrier fluid, fluorescent detection fluid, and the wash fluid are loaded into syringes which are placed in syringe pumps, and pumping commences at the desired flow rate. For experiments done up to this point, the

fluorescent antibody inlet is infused with PBS and the beads are collected from the device outlet for off-site fluorescence detection, as described below.

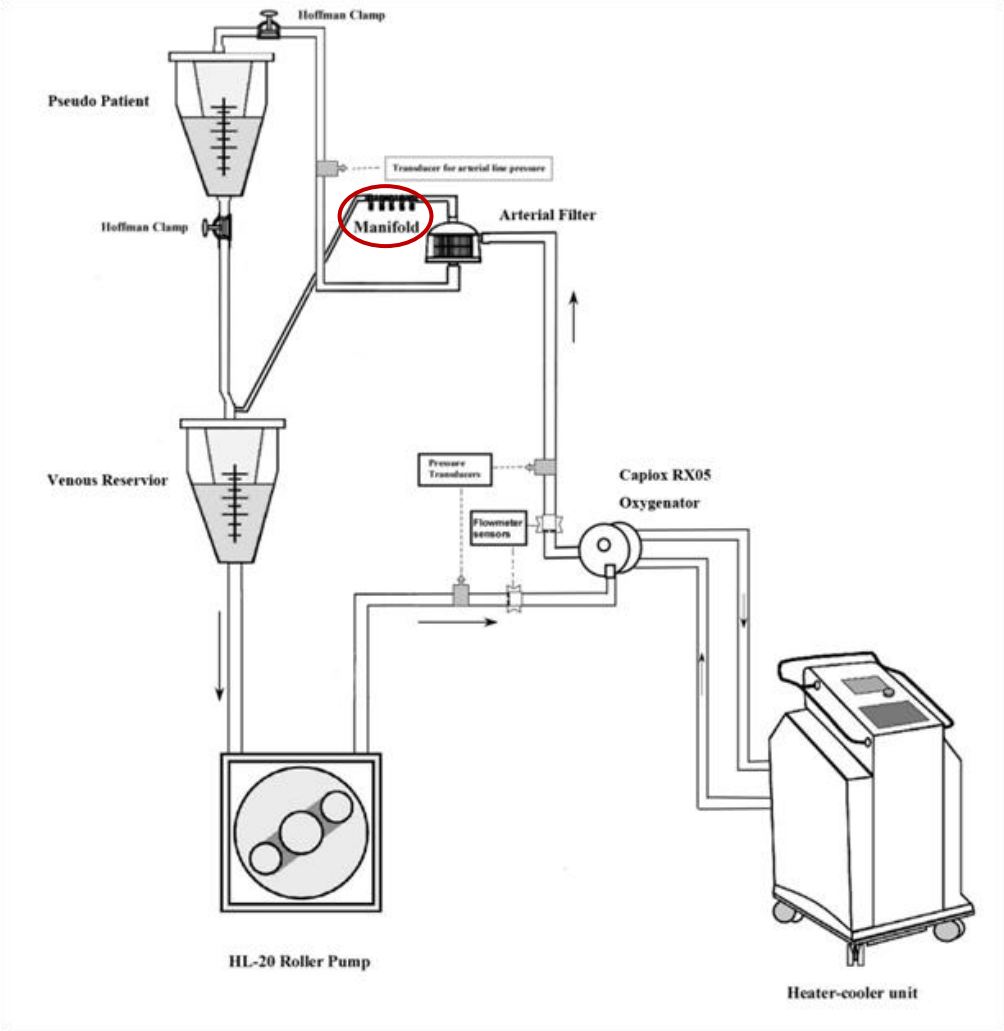

Figure 4-7: Schematic of simulated CPB circuit using human donor blood. The sampling manifold, from which the sample stream is sourced, is encircled

The sample inlet is connected using the system described in section 4.5.2 above. The sample stream is sourced from the sampling manifold, shown in Figure 4-7. A port on the manifold is connected to the inline microfiltration device, and the filtrate outlet is

connected to the inlet of the peristaltic pump. The pump outlet is connected to the sample inlet port of the micro-immunoassay device, and the valve, damper, and pressure sensor are connected to the ports downstream of the inlet port. As mentioned above, the damper syringe is pressurized by a second syringe to expedite the buildup of pressure in the damper, which must reach the setpoint for the flow to stabilize at the desired rate. When the flow stabilizes, which can be determined using the real time pressure monitoring output from the pressure controller, the device begins to properly incubate the microbeads for the assay. Detection can begin after stabilization occurs and the device lag time has elapsed (section 2.2.3, "Assay measurement lag time"). This allows beads which entered the device before flow stabilization occurred to be flushed out.

4.5.3.1 Off-site fluorescence detection methods

The off-site fluorescence detection method is used when there is no detection equipment available during the experiment. This method can use two different types of fluorescent tagging, either on-chip or off-chip. The first incubation stage (analyte binding to microbeads) is performed on-chip in a continuous flow environment in both cases. The incubated beads are collected in Eppendorf tubes as they flow from the detection outlet. Bead collection is generally done in 15 or 30 minute intervals, which reduces the sampling rate of the device, as described in section 2.2.4. When the fluorescent tagging is done on-chip, the fluorescent secondary antibody is infused into the chip as described in section 3.3.1. For off-chip incubation, the fluorescent secondary antibody stream is replaced with PBS, so no binding occurs during this stage. After collecting the primary-incubated bead samples, fluorescent tagging is performed using a bench-top incubation with the same duration as the on-chip incubation.

4.5.3.2 On-site fluorescence detection with integrated flow cytometer

To enable continuous CPB inflammation monitoring, a modified flow cytometer can be set up along with the micro-immunoassay device and related equipment adjacent to the CPB circuit. The incubated beads would flow directly from the microdevice into the flow cytometer. The fluorescence data is recorded and the analyte concentration can be calculated in real time. This method has not yet been tested.

4.5.4 Experimental results from preliminary CPB integration experiment

The microfluidic immunoassay was integrated with a simulated CPB circuit for an initial test. This test included the integration of a microfiltration device to provide blood plasma for analysis in real time (detailed in section 4.5.2.1). Off-site fluorescence detection was performed with off-chip fluorescent tagging, as described in section 4.5.3.1. The peristaltic pump was used to draw blood plasma from the filtration outlet of the microfiltration device at a flow rate of approximately 10 μl/min, which was stepped down to 1 μl/min at the micro-immunosensor's sample inlet using the pressure control system described previously. Some cavitation was evident in the plasma sample tubing, but all bubbles were skimmed off into the damper connection tubing and ultimately floated into the damper's air column, thus not entering the sensing portion of the microdevice. Photographs of the microdevice during the integration experiment are shown in Figure 4-8. The device was placed on a microscope for visual inspection during the experiment.

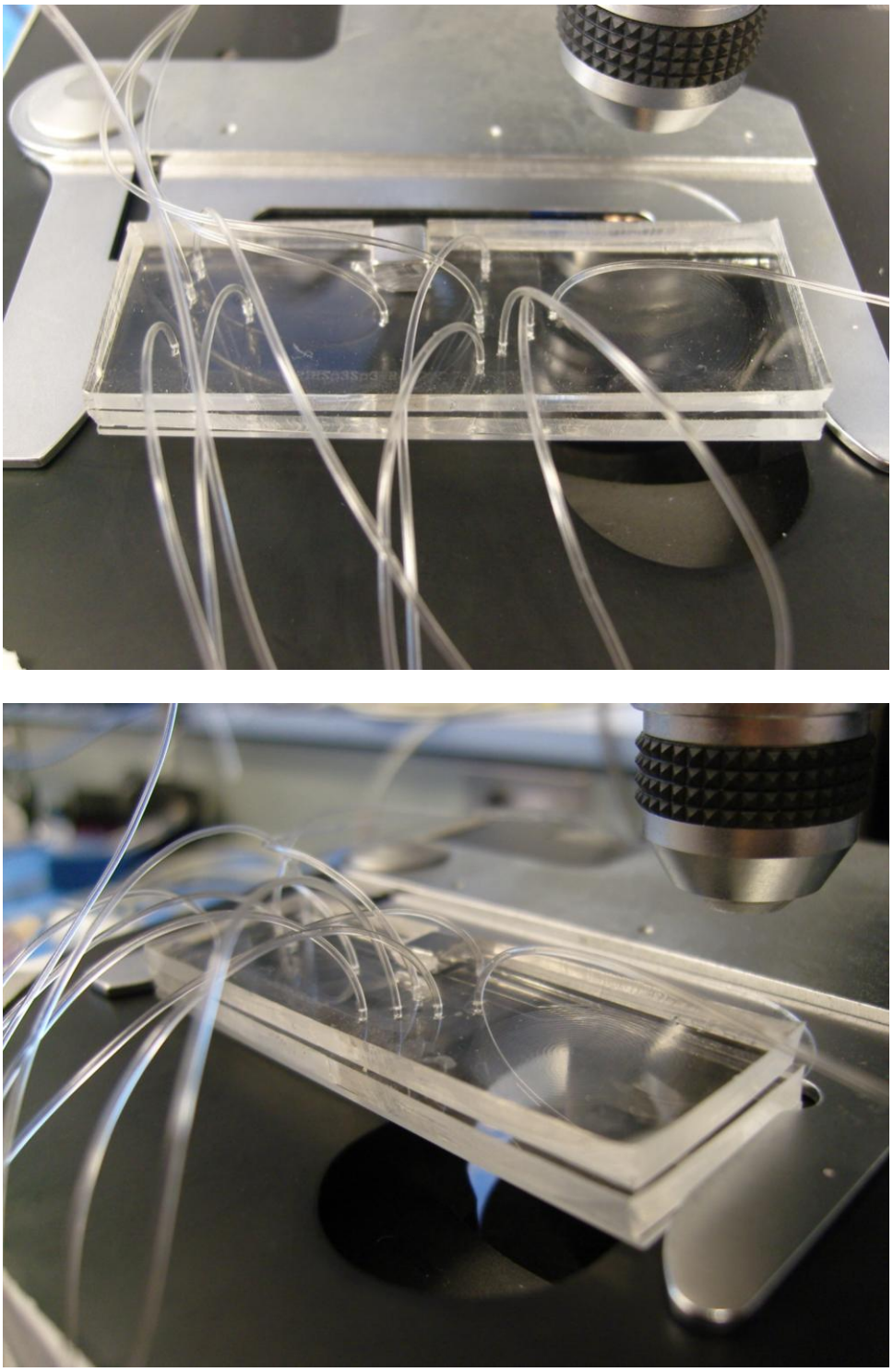

Figure 4-8: Photographs of the microfluidic immunoassay device with spiral incubation channels during CPB monitoring experiment

Measurements began after 300 minutes of CPB circulation time, and samples were collected every 20 minutes for 160 minutes. The data show the expected increase in complement C3a concentration over time, with values in the expected range, however these results have not been compared to traditional assay results from the same blood samples (Figure 4-9). A calibration of the device with calibration standards was performed off-site by running the same microfluidic device which was used with the CPB, and fluorescently tagging the beads at the same time as the incubated beads from the experiment.

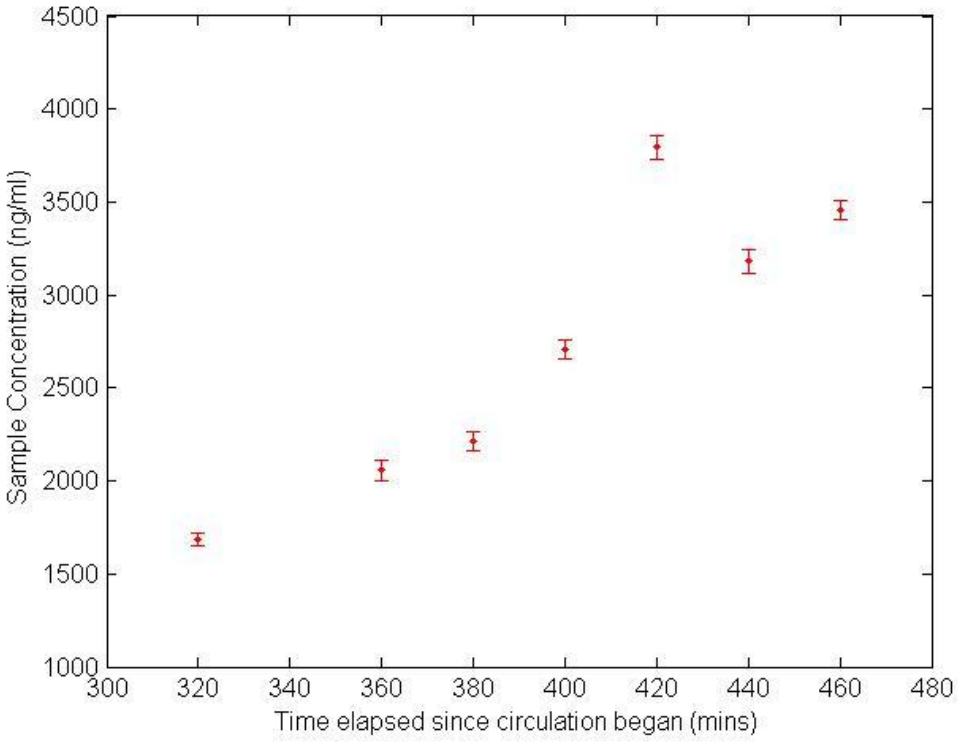

Figure 4-9: Temporal tracking of C3a concentration in an integrated plasma filteration and bead incubation device. Fluorescence labeling and flow cytometry of beads were conducted one day after antigen labeling of the beads in the microdevice. The second time point was corrupted due to a problem with the flow cytometer and is thus excluded

5 MULTIPLEXED DETECTION WITH LUMINEX xMAP ASSAY AND RELATED DESIGN OPTIMIZATION

5.1 Purpose

The Luminex xMAP system is a patented technology which enables multiplexed analyte detection using a mixed magnetic bead population. The assay is most commonly performed on the bench using traditional liquid handling techniques with either centrifugation or filter plates to allow washing of the microbeads between incubation stages. When this research began in 2007, there were no magnetic bead sets available with this technology. Recently, Luminex and some xMAP licensees such as Bio-Rad have begun marketing magnetic bead arrays for some analytes. Of most importance to this research is the Bio-Rad Bio-Plex Pro Human Cytokine, Chemokine, and Growth Factor Assay. This reagent kit allows multiplexed detection of up to 50 analytes, many of which are relevant to the inflammation processes of interest for mechanical circulatory support and spinal cord injury. While the beads supplied by Bio-Plex are slightly smaller than those for which the microdevice was optimized (6.5 μm versus 8 μm), through testing it was shown that the microfluidic bead actuation function similarly with either microbead type. The off-the-shelf reagent system has also proven to be more refined than the custom reagents which were previously being used. This is evident in both the stability of the reagents in storage as well as the significantly assay higher sensitivity which has been achieved. The reagents can be customized if necessary to provide detection of any analyte for which a pair of detection antibodies is available. Due to the superiority and increased robustness of the Bio-Plex reagents based on Luminex xMAP

technology, it was decided to focus further efforts entirely on accommodation of these products. In order to demonstrate multiplexing, a duplex assay was used in all experiments which detected IL-6 and TNF-α.

5.2 Assay principle

Multiplexing with Luminex xMAP is accomplished using a fluorescent color-coding system where two additional fluorescent tags are added to each bead to code for a specific analyte. The intensity of each of these fluorescent tags is used to locate the microbead on a two dimensional grid such that it can be identified during detection. This coding scheme is illustrated in Figure 5-1. The Luminex assay uses a three-stage incubation approach. The first stage captures the antigen of interest by again incubating the monoclonal antibody coated microbeads with the sample, where the amount of bound antigen on each microbead after incubation is correlated to the sample concentration. In the second stage the beads are incubated with a biotinylated secondary antibody to the antigen of interest. Finally, in a third stage the microbeads are incubated with a streptavidin-phycoerythrin (PE) conjugate to fluorescently tag to detection antibody. The three-stage microbead assay is depicted in Figure 5-2. As in the two-stage assay, the fluorescent intensity of each bead is correlated to the antigen concentration in the sample. The sample concentration, as well as the color-coded identifier, are detected via flow cytometry.

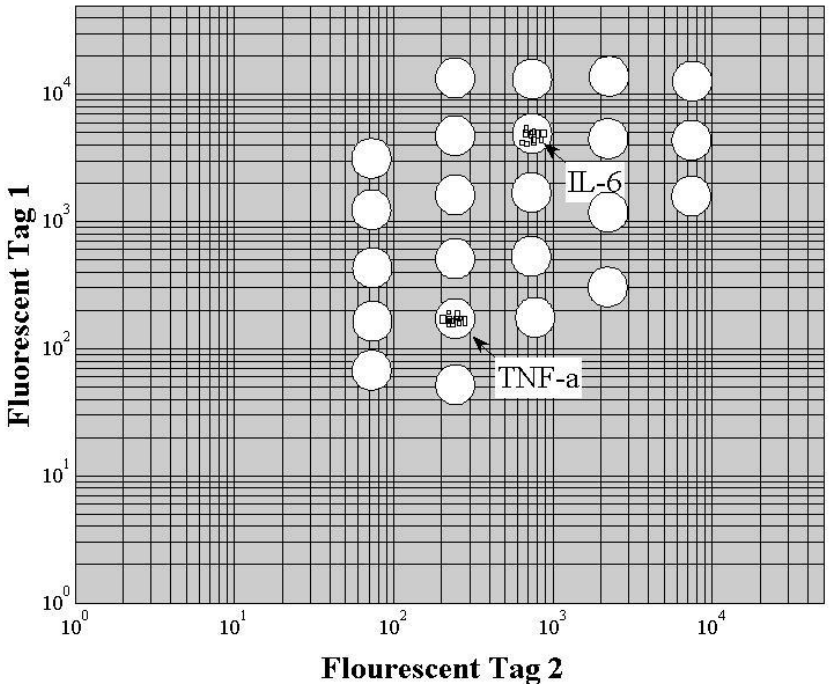

Figure 5-1: Representative fluorescent coding used in a Luminex xMAP assay. Each circle represents a potential gating region for fluorescent detection of the analyte specifying colors. In this case a duplex assay is shown, where fluorescent particle events are detected in the two regions of interest. (Figure by Ian Johnston)

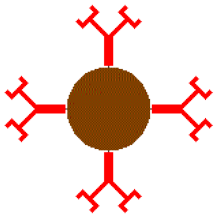

Prior to the assay, the stock bead is already color coded for multiplexed detection and conjugated with the specific monoclonal antibody

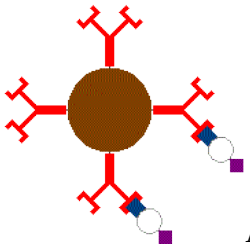

After the first stage of the assay the bead has accumulated the antigen of interest in an amount that is proportional to the sample concentration

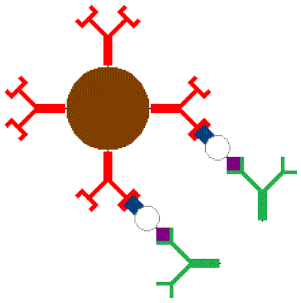

After the second stage of the assay, the bead-bound antigen are conjugated with a biotinylated detection antibody

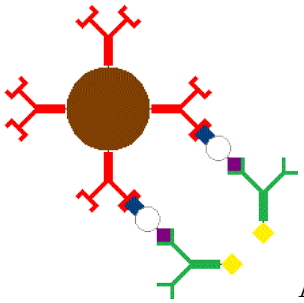

After the third and final incubation stage, a streptavin-conjugated fluorescent phycoerythrin tag is bound to each detection antibody

Figure 5-2: Microbead incubation schematic for Luminex xMAP

5.3 Fluorescence detection

For all Bio-Plex experiments, the incubated bead samples were plated in standard 96 well plates, and interrogated using a Bio-Plex 200 flow cytometer. The machine uses two lasers (green 532 nm Nd-Yag, and red 635 nm laser diode) for detection of three fluorescent channels and one side scatter channel for doublet discrimination. All detectors use 15-bit analog to digital conversion. There is a 15-bit doublet discriminator based on forward scatter which was set to an inclusion window of 8,000 to 24,000. Each sample infusion was 50 µl, and a minimum of 50 beads per analyte region was required (50 for TNF-α plus 50 for IL6). All experiments used the high sensitivity PMT mode except the incubation time test, which used the low sensitivity mode to achieve a wide dynamic range.

5.4 Bench top validations

5.4.1 Incubation time test

In order to determine the feasible incubation time range of the Bio-Plex assay, the assay was tested with varying incubation times using an otherwise standard procedure to characterize the binding kinetics and the resulting relationship between assay sensitivity and incubation time. The procedure from the assay manufacturer's instructions (72) was followed exactly, with the filter plate washing method, and using the provided assay standards. The incubation times were adjusted by delaying the addition of reagents to wells. For instance, in the first incubation stage, the standards were added at 0 min., 15 min., 20 min., 25 min., 28 min., and 29 min. The wash step then proceeded simultaneously for the entire plate. This procedure was followed for all three incubation

stages. The fluorescent detection method described in Section 5.3 was used for quantification. The results are displayed in Figure 5-3.

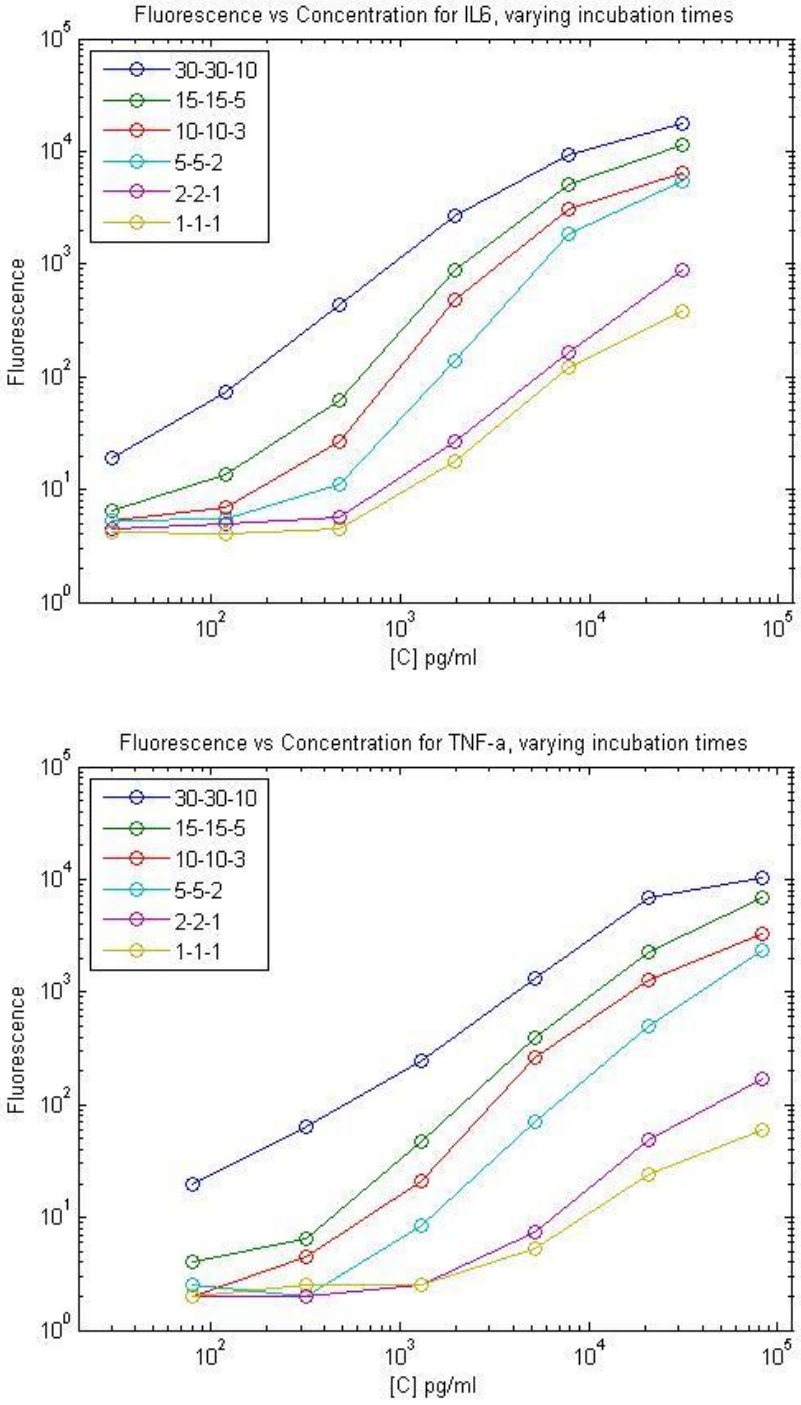

Figure 5-3: Incubation time test with varying times and concentrations, IL-6 and TNF-α

5.4.2 Off-chip benchmark assay

In order to provide a benchmark to assess the performance of the microdevice, an analogous procedure to the on-chip assay was performed off-chip. 100 µl of each microbead stock is mixed in a microcentrifuge tube which serves as the incubation vessel, washed twice with Wash Buffer, aspirated and left unsuspended. 400 µl of antibody diluents is added to 50 µl of each detection antibody in a microcentrifuge tube. In another tube, 500 µl of assay buffer is mixed with 5 µl of PE stock solution. 50 µl of each standard is added to each incubation tube and the solution is mixed with a pipette. After 5 minutes the incubation tubes are diluted with wash buffer and washed twice via centrifugation and left unsuspended. For the second incubation stage, 50 µl of the prepared detection antibody solution is added to each tube, mixed, and incubated for 5 minutes. The same wash procedure is used and finally 50 µl of the prepared PE fluorescent tag solution is added to the tubes and incubated for 5 minutes. After two more wash steps, the microbeads are suspended in 125 µl of assay buffer, vortexed, and plated. The fluorescent detection method described in Section 5.3 was used for quantification. The data from the off-chip assay are shown in Figure 5-4.

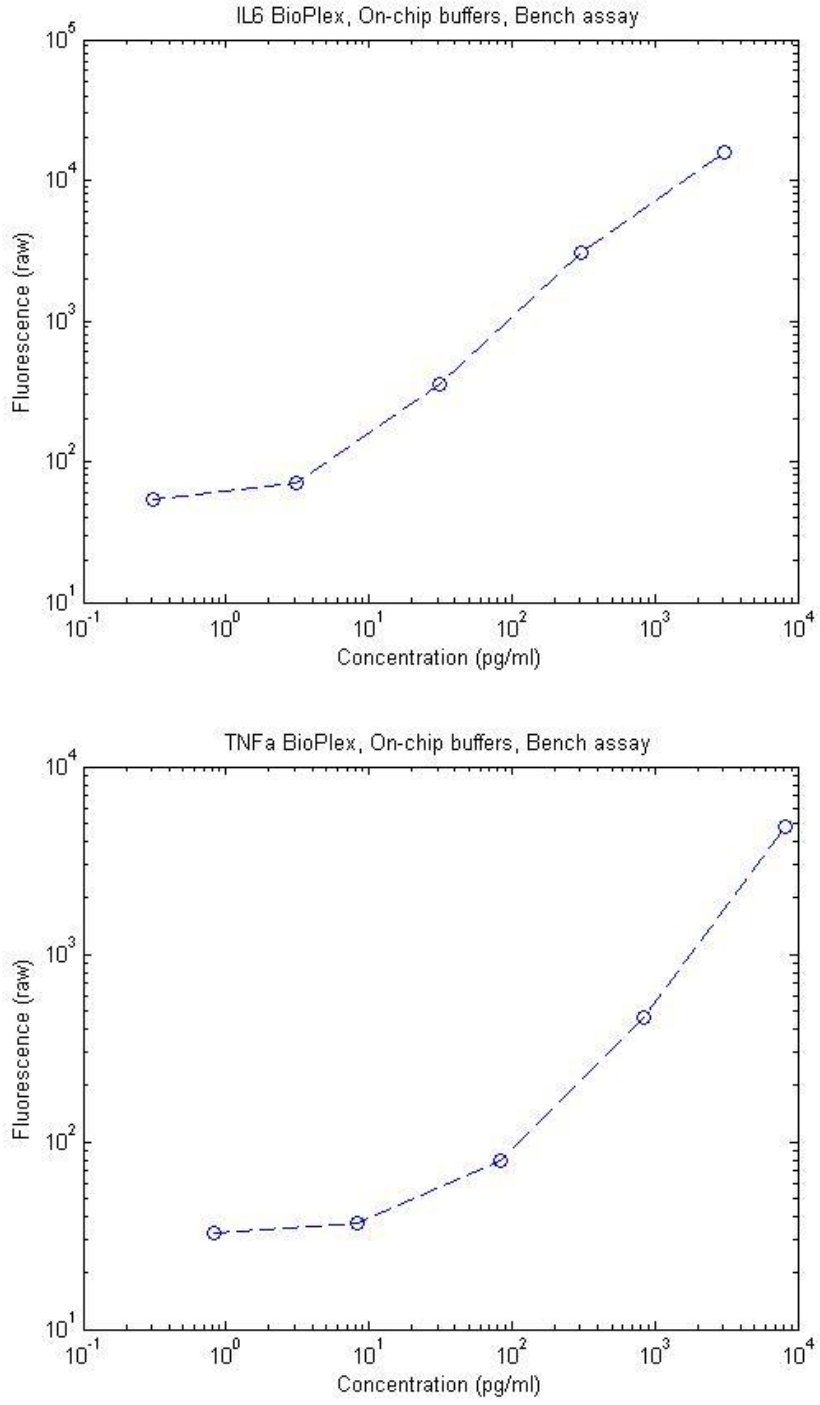

Figure 5-4: Off-chip benchmark assay for IL-6 and TNF-α

5.5 Necessary design adjustments

The primary design adjustment that is required to accommodate the Luminex xMAP assay is the addition of a third processing layer. The two-layer design has inherent universality such that in theory any number of layers can be added on top. The difficulty arises in finding space on the 75 mm x 25 mm platform for the additional input and output ports. The addition of the third layer was feasible within the available space, however adding any more layers would likely be too difficult without a larger chip footprint.

An important consideration when adding additional layers is the flow resistance balancing on each layer. The streams entering the lowest layer see the resistance of a single incubation spiral, and thus the waste outlet it matched with a resistance matching spiral channel of equal resistance to the incubation channel. However, each additional layer adds an additional incubation length to the forward-looking flow resistance, and the waste spiral designs on upper layers must take this into account. For Layer 2, the total incubation resistance is double that of Layer 3 (the lowest layer), so the waste spiral channel width was cut in half to double its resistance. For Layer 1, the resistance is three times that of Layer 3, or 1.5 times that of Layer 2, since the flow will traverse three incubation channels. The waste outlet on Layer 1 has the same channel width of Layer 2 (half of Layer 1), but is 50% longer. The three-layer device layout is shown in Figure 5-5.

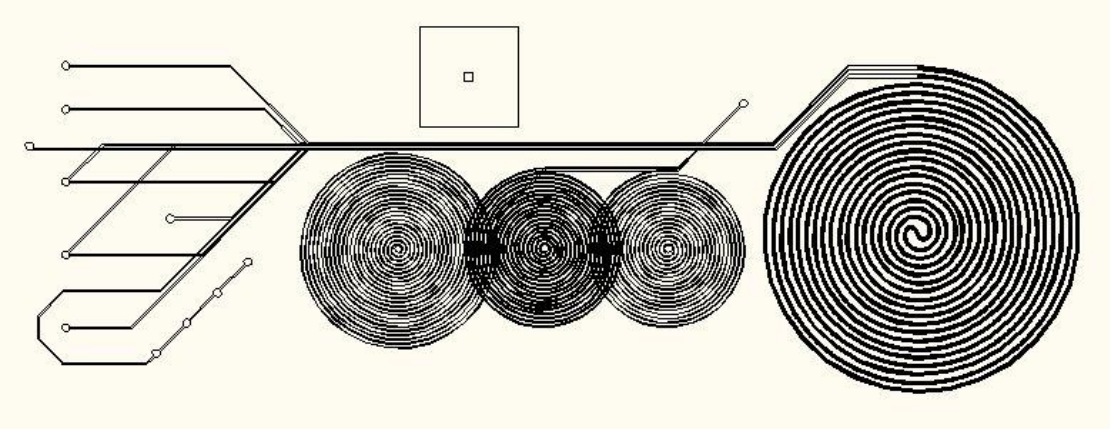

Figure 5-5: Channel layout of the three-layer design

5.6 On-chip experiments

5.6.1 Reagent preparation

The reagents for the on-chip assay are prepared differently from the assay instructions to optimize them for microdevice infusion. 100 µl of each microbead stock is mixed in a microcentrifuge tube, washed twice with Wash Buffer, and suspended in 600 µl of Ficoll-Paque Plus (GE Healthcare) for density matching such that the microbeads do not sediment after vortexing. 75 µl of each detection antibody stock is mixed with 600 µl of antibody diluent. 6 µl of phycoerythrin fluorescent tag stock is mixed with 600 µl of Assay Buffer. The provided wash buffer is used for the microdevice wash stream.

5.6.2 Experimental procedure

The device is first infused via syringe pump with a mixture of PBS with 0.01% BSA until all channels are filled. The reagents are then infused using two syringe pumps, one for the magnetic microbeads, detection antibody, fluorescent tag, and wash buffer, and a second for the sample syringe which is replaced repeatedly throughout the experiment.

All flow rates are 1 µl/min. After a new sample syringe is attached, there is a 20 minute flush time, followed by 15 minutes of bead collection. The collected beads are diluted with 100 µl of Assay Buffer and transferred to a well plate for fluorescence quantification. Samples were created by serial dilution of the provided Bio-Plex standards, and are in the general range of 1 pg/ml to 1000 pg/ml.

5.7 On-chip multiplexed assay results and discussion

The principle goal of these experiments is to show that the microdevice can provide the same measurements as the bench top assay, but with total automation of the microbead processing. The bench top (off-chip) assay was designed to directly mimic the on-chip assay in terms of the incubation times, buffer solutions, and detection method. The on-chip and off-chip methods did ultimately provide similar measurements, with some variation as is expected with these types of assays. The results are compared in Figure 5-6.

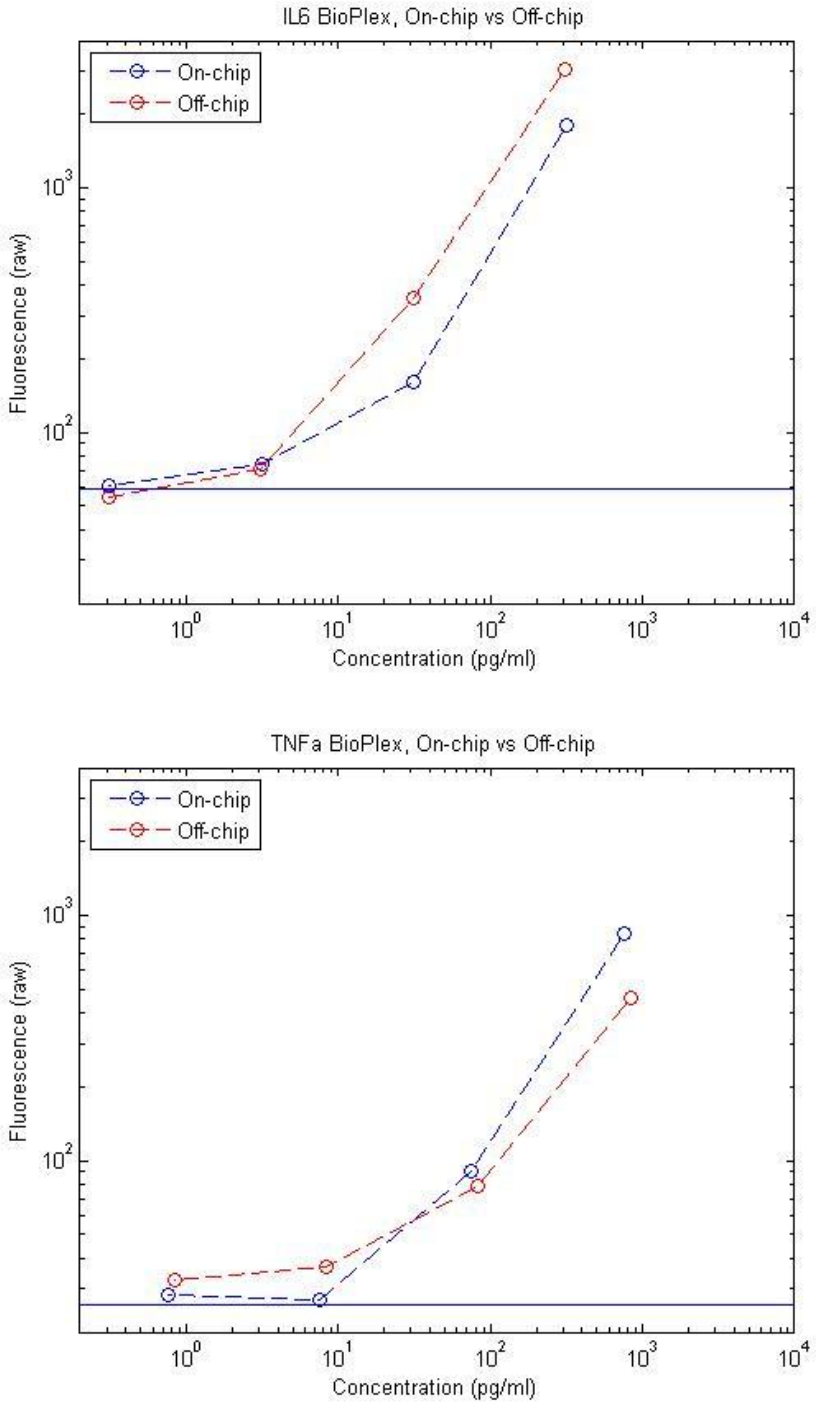

Figure 5-6: Comparison of on-chip and off-chip Bio-Plex data for IL-6 and TNF-α multiplexed. The solid horizontal line represents the negative control level for the on-chip data.

A second important experimental goal was to show that the device could respond identically to step changes in sample concentration in the increasing and decreasing directions. This experiment also shows the lag time of the microfluidic assay in its current state. While the theoretical lag time of the device is in the range of 15 to 20 minutes, the device as built seems to have a lag time near 45 minutes (Figure 5-7). The swept volume of the outlet tubing and layer transfer holes are expected to account for at least 8 minutes of this additional lag time. It has yet to be determined if the remaining lag time in the system is due to additional swept volume delays, or other aspects of the physical system such as axial mixing of samples. However, the apparent step change in output fluorescence is a sign that axial mixing is minimized and that accurate tracking of sample concentration is feasible. The addition of on-chip detection and other optimizations will significantly reduce the lag time of the assay.

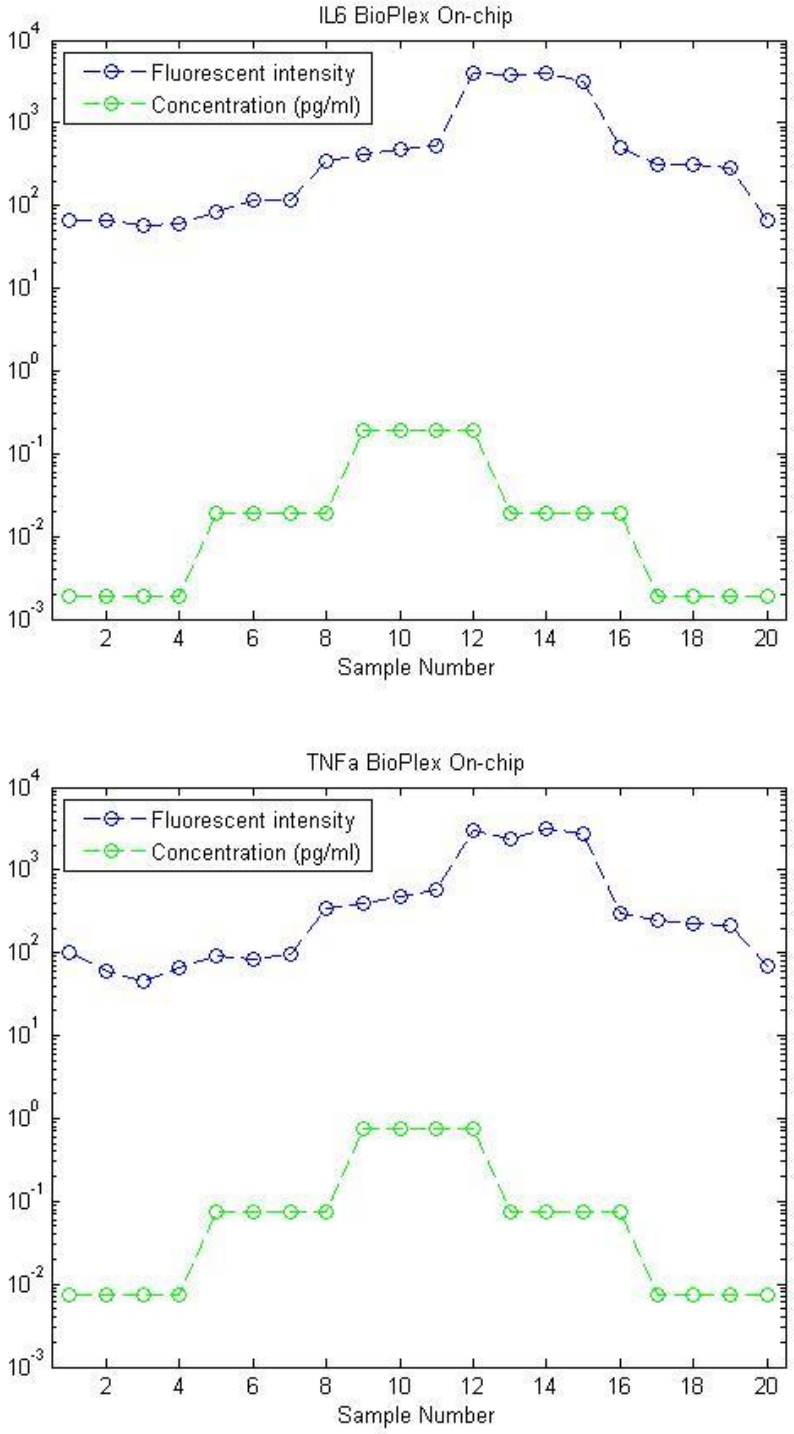

Figure 5-7: On-chip incubation data for Bio-Plex assay with batch collection of beads every 15 minutes. The step-wise change in bead fluorescence due to the step-wise change in sample concentration is apparent.

5.8 Additional applications enabled by xMAP integration

Given the increasing popularity of xMAP assays in laboratory research, the microdevice assay could provide benefits for current users who manually process the assays. The microdevice is capable of providing automated processing of discrete samples, as has been done in most of the experimentation which has been described. This type of automation would have the benefit of reducing labor costs, reducing the training required to perform assays, and avoiding human error. With optimization of the supporting equipment for the microfluidic assay, it will also reduce the volume of reagents used per sample. Furthermore, there are clinical applications where a single shot, automated, in-house test would be preferable to sending samples for traditional outside laboratory analysis.

For discrete sampling of multiple samples, the samples can be loaded consecutively to increase the turnaround time for multiple samples. For example, if each sample is infused for 2 minutes and directly followed by the next sample, the total assay duration would equal the assay lag time for one sample plus 2 minutes for each additional sample. Thus, if the lag time for one sample is 20 minutes as described above, the time for 10 samples would equal

Equation 5 $$\mathbf{20\,min} + (\mathbf{10} - \mathbf{1}\,\boldsymbol{samples}) * \mathbf{2}\,\boldsymbol{min/sample} = \mathbf{38}\,\boldsymbol{min}$$

The detection recording would be timed such that each 2 minutes detection period would correspond with the appropriate sample number.

If higher sensitivity is needed, the incubation times can be lengthened to as much as 25 minutes per stage by reducing the flow rate, at the expense of increased lag time, which will provide detection limits below 1 pg/ml. For some applications, such as

monitoring yield in bioproduction, the expected protein concentrations will be at least 100 times greater than typical clinical concentrations, and can be as much as 10^6 times greater for high yield processes. In these cases, the incubation times can be reduced to below 1 minute per stage. If the incubation time must be reduced without increasing the sample flow rate, the spiral incubation channel can be shortened as necessary to reduce the channel length.

5.9 Optimized microfabrication technique

5.9.1 Photolithography

Due to the complexity of the 3-layer spiral channel device, the standard lithographic fabrication technique had too high a failure rate. The major problems are related to adhesion of the SU-8 photoresist to the glass or silicon substrate, and bubbles in the photoresist overlapping the device channels, which is exacerbated by the high feature density of the design. Two methods were found to mitigate the problem of bubbles in the resist. First, a higher spin coating speed helps to break down bubbles, even if it requires switching to a higher viscosity formulation. At least 2000 RPM is preferable. Previously, SU-8 2010 was being spun at a spin rate of 1000 RPM to produce a ~20 µm layer. The design was altered to a 40 µm target channel depth in order to reduce the overall system pressure. This allowed the use of SU-8 2025, a higher viscosity formulation, but the spin rate was increased to 2000 RPM. The result was a reduction in bubbles in the layer. The second method to address bubbles is to pour the entire required volume of photoresist from the bottle in a single motion. When the resist is poured more slowly there is a tendency to form bubbles in the layer being poured. The pour should be abruptly terminated by interrupting the flow with a lint free wipe, otherwise the trailing drops will

create bubbles. Popping of bubbles with a needle is possible, but it is time consuming and unreliable.

An alternative method for generating masters with photolithography is through deep reactive ion etching (DRIE). This method allows the use of a more conventional photoresist, such as Shipley 1818, on a silicon wafer which is then etched to the appropriate feature depth. This method is costly, so it is only recommended for a somewhat finalized design. Furthermore, the wafers can be easily cracked during soft lithography de-molding.

It was ultimately found that the best overall method for prototype master fabrication is SU-8 deposited on aluminum substrates. The substrates were prepared by cutting 0.125 inch thick 7075 aluminum plate into rectangular pieces with dimensions of 3 inches by 2.5 inches. To achieve a smooth final finish on the bonding surface of the PDMS chip, the plates must be polished using a multi-step mechanical aluminum polishing procedure. The degree of polishing has no effect on the device functionality. The adhesion of SU-8 on this type of substrate was empirically found to be at least as good if not better than adhesion to silicon. Furthermore, the plates cannot be broken. Approximately 50 molding cycles should be possible with this method before the SU-8 channel corners begin to develop cracks, reducing the quality of the final channels, although not completely interrupting the functionality of the devices. There has yet to be an adhesion failure on one of the masters.

5.9.2 Soft lithography Procedure

While traditional soft lithography has been used to produce prototype devices, the complexity of this device leads to a high failure rate for this minimally controlled manual

process. For comparison, this device's three layers taken together have a total channel length of more than 2 meters. Fabrication is further complicated by the large area of the chip which is populated with critical features, leading to a high likelihood of production anomalies overlapping with features. Common problems leading to device failure have been related to localized bonding failures, unexplained leaks between adjacent channels, chunks of PDMS becoming dislodged and sticking in the channels leading to clogging, foreign debris, and imprecise port punching which results in leakage. Despite these problems, the project has made slow progress by attempting to control the relatively uncontrollable soft lithography process as much as possible. Through extensive experimentation, the following procedure has produced the best results.

- Mix PDMS 10 parts base and 1 part crosslinker (e.g. 55g + 5.5g)
- Pour PDMS, fill to appropriate depth (Extra height negatively affects hole punching)
    - Layer 1: 4.25 mm +/- 0.25
    - Layer 2: 2.25 mm +/- 0.25
    - Layer 3: 3 mm +/- 0.5
- Place in vacuum chamber to remove air from between spiral features (important)
- Cure for 2 hours at 65 C
- Punch transfer hole on lower layer only, use 22 gauge blunt tip needle (sharpen needle with .02" drill bit)
- Punch port holes in top and bottom, use 19 gauge blunt tip needle (needle must be sharp to avoid cracking PDMS which will cause leakage)
- Clean
    - Use clear tape to remove debris

    - Rinse bonding surfaces (bottom of top layer and top of bottom layer) with acetone, then isopropanol, then DI water
    - Dry both part thoroughly with filtered compressed air
- It has been shown that cleaning and bonding in the cleanroom results in a significant reduction of debris in the device
- Bond
    - Treat bonding surfaces with corona discharge
    - Align top over bottom, lining up transfer hole and channels
- Place in oven at 100 C for 1 hour
    - There is evidence that bonding at 65 C for 30 minutes will reduce the brittleness of the PDMS resulting in smoother ports
- Punch existing holes on lower layer through top layer
    - Punch must be sharp and clear every time
- Repeat cleaning procedure for bonding surface of PDMS and glass slide
- Repeat bonding procedure, if necessary use binder clamps to hold the edges down (if the PDMS is warped), or use weights

6 CONCLUSION

6.1 Overview

This work has culminated with the development of a novel, unique, patent-pending biomedical device. Significant progress has been made toward the original application goals, and additional applications have been identified. While not all aspects have been entirely integrated due to cost constraints typical of early stage technology development, it has been demonstrated experimentally that the design can enable all of the originally specified features: autonomous operation, continuous monitoring, near real-time sensing, high sampling rates, multiplexing, and low sample volume consumption. The following sections are focused on a broader view of the technology, including additional technical development goals, intellectual property, and considerations for commercialization.

6.2 Multiplexing and off-the-shelf reagent availability

The multiplexing feature deserves special consideration, mainly because it was enabled through an outside influence. The decision by Bio-Rad to market a magnetic version of their assay reagent kits during the course of this research was to some degree a lucky break. However, it is significant in that it shows the direction toward which the biomedical diagnostics industry is moving. The company claims to have added the magnetic feature in order to enable additional assay automation processes, yet at the time when these products went to market the company did not offer any automation solutions using magnetism.

6.3 Remaining technical challenges

Development and characterization of the microfluidic assay will not be complete until it is integrated with a flow cytometry system. Both continuous monitoring as well as discrete sampling will be enhanced by an integrated detection system. The principle concerns for flow cytometry integration are hydraulics and optics. Two options stand out for the purpose of showing proof of concept. First custom flow cytometers are available from a company called Cytek. These machines offer the simplest option for hydraulics because they allow externally driven flow. In this case the optics would have to be specified to match the Luminex system, which may or may not achieve the same sensitivity as the Bio-Plex cytometer. A second option is to modify a Bio-Plex machine. In this case the optics are already optimized, but the hydraulic system would require complete customization, and the level of difficulty of this work has not yet been clarified. In either case, the system will ultimately require custom electronic hardware and software to control the assay, read the fluorescence data and process the results. For proof of concept, there are various methods to extract data from these machines with time as a parameter, however real-time results would not be possible without a custom electronic system.

In order to fully integrate the automated assay, a specialized pumping system will be required. For the reagent streams, two options stand out. Pneumatic pumping is an inexpensive option but will require precise pressure control, and the flow balancing through different areas of the chip will have to be thoroughly tested and characterized to ensure that it is correct and reliable. The second option is a syringe system similar to what is used in robotic liquid handling machines, as well as in the Bio-Plex machine.

This type of system utilizes stationary glass syringes to infuse liquids and then pump at a controlled flow rate. This technique is probably more expensive, however ensuring accurate and stable flow is much more straightforward. For sample infusion, a syringe or pneumatic system is also applicable for discrete sampling. For continuous infusion from in vivo sources, an inline pump is required. A peristaltic pump is an inexpensive option which has been proven effective. Other more exotic pumping systems may also suffice for inline pumping.

There is some evidence that flow balancing can be affected by the viscosity of the fluids. This effect is generally controllable through optimization of the channel geometry. However, when the inlet flow is controlled based on pressure, such as is the case for the peristaltic infusion system described in Section 4.5.2, variations in the flow balance may occur during the course of the assay especially due to temperature changes in the infused fluids. The effects of viscosity on flow balancing are clearly evident when one considers that this effect alone can be used in practice as a metric for viscosity (73). Ultimately, changes in viscosity due to temperature variations may be mitigated if the commercial equipment developed for the assay includes refrigeration to preserve the reagents and samples, since this would maintain the temperature of the fluids in a tightly controlled range.

6.4 Additional future work

As described in Section 3.3.2, the movement of microbeads through the incubation channels is not entirely uniform. This occurs due to edge effects in the channel, where flow streamlines closer to the walls have lower velocities than those near the center of the channel. While bead to bead variations are inevitable even in bench top processing, an

improvement in uniformity will always be beneficial in reducing the deviation in fluorescence between microbeads incubated in the same sample. A smaller deviation allows a smaller number of microbeads to be included in the ensemble average for each measurement without affecting the accuracy of the result. This reduction can in turn reduce assay turnaround time, and it also increases the effective sampling rate in continuous monitoring mode due to a reduction in the time window for the moving average. Thus, one possible area of improvement for this technology would be to reduce the variation in microbead velocity, either passively through hydrodynamic considerations, or actively by manipulating all of the microbeads into desired streamlines.

6.5 Novelty and intellectual property

The technology which has been described is currently pending international patent protection as a Patent Cooperation Treaty (PCT) filing. The application (PCT/US09/38880), entitled “Methods and Related Devices for Continuous Sensing Utilizing Magnetic Beads”, was filed on March 31, 2009, and entered the United States National Phase (U.S. Patent Application Serial Number 13/123,547) on April 11, 2011. While the newest embodiment of the device has been optimized since the original design as shown in the filing, the same fundamental principle controls the device operation in all of these designs. At this time there remains only one competing technology which presents a similarity to this design. The design by Pamme et al. described in Section 2.3.3 shares some of the same features, such as the use of magnetic beads and permanent magnets with a microchannel. The key differences which establish the novelty of our design as compared to the Pamme design amount to the concepts of permanence and continuity. In the Pamme design, each manipulation event of a microbead between two

reagent streams is an inherently transient event. A single trajectory defines and necessitates the movement of microbeads across all of the reagent streams. In contrast, with our design each microbead manipulation to a new reagent stream leads to permanent residence of the bead in that stream until a separate manipulation event with a new trajectory occurs. For this reason, our design uses a discontinuous, or step-wise, bead manipulation approach with multiple incongruent trajectories. This is in contrast to the continuous trajectory employed in the Pamme design.

6.6 Additional applications

Broadening applicability is a common theme in long term engineering research and development projects. This particular project began with high specificity, where the solution followed directly from the requirements for a single problem. Once the proof of concept was demonstrated, and a clearer idea of the technical possibilities emerged, the solution revealed further problems which could be addressed. A broadening problem set is an important part of the risk/reward structure of technology development. In this case the risk of developing a solution for a niche problem may be outweighed by the previously unknown additional problems that can be addressed. An ideal outcome would be for the developed technology to encounter a substantial market in its original intended application, as well as a periodically growing set of additional substantial market applications. It is my belief that there is some potential for the present technology to achieve this level of significance, but it will depend on the ultimately achievable assay performance as well as cost structures each of the markets.

Some additional applications have been identified during the course of this work. One possible market is general laboratory automation. Automation for microbead assays has

been addressed by the industry through robotic liquid handling in similar ways to plate based assays such as ELISA. The microfluidic assay may offer benefits over traditional robotics, especially in terms of the cost and complexity of the supporting equipment. There are also examples of clinical applications aside from mechanical circulatory support monitoring where this technology could offer a value. It has been suggested that an automated fluorescent immunoassay for early markers of Type 1 Diabetes Mellitus would provide advantages over the common radioimmunoassay currently in use. There may be additional applications in the diagnosis or monitoring of other autoimmune diseases. In addition to disease markers, the device could be used to detect therapeutic agents to study bioavailability. It is expected that numerous additional laboratory and clinical applications of this technology will emerge.

6.7 Commercialization

Aside from technical challenges, the key to commercialization of this technology will be to identify a market with a high probability of adoption and low barriers to entry. This will most likely be a clinical application that does not require FDA 510(k) approval. Currently, a variety of Class I and Class II medical device applications are listed as exempt due to the FDA Modernization Act of 1997 (74), and these areas may be appropriate for an initial market approach. Once a market footing is achieved, additional applications of the technology can be added based on the market size and the potential markup based on the prices of competing technologies. The hardware and device design is likely to carry over significantly between different applications.

Another consideration for an initial market approach is the complexity of controlling the assay. While it has been shown that a continuous sample infusion from a time-varying

source can be controlled using a closed-loop algorithm, a discrete sample flow control system based on syringe pumping would be significantly simpler and more robust. Permanent syringe plungers can be incorporated into a piece of equipment, while the chip itself can be molded with cylinders to receive the plungers. This arrangement would reduce or remove the need for cleaning of syringes between uses. As stated above, the benefit of syringe based control is that achieving stable flow is trivial with a simple electromechanical system. This type of pumping circumvents the problems associated with controlling flow of non-newtonian fluids and accounting for temperature and other viscosity changes. Furthermore, because the microfluidic system is designed for equal flow rates at all inputs, a single driving motor could be used for all syringes. Thus, an ideal first application of this technology may be a system for single-sample point-of-care testing where the reagents and sample are loaded onto the chip into integrated syringe cylinders, which need only be a few millimeters in height, and plungers are driven by a single stepper motor to drive the reagents thus performing the assay processing. A test such as the one mentioned for diabetes biomarkers could have reagents pre-loaded on the chip and sealed with a peel away plastic cover. Standards can be loaded in series in a sample inlet channel with bubbles of air or another hydrophobic fluid separating them, and the sample can be loaded into the cylinder behind the standards, so that the standard curve and sample interrogation and processed sequentially with a single motion of the actuating syringes. This relatively simple system would be completed by integrated flow cytometry optics, preferably with the chip acting as a flow cell. The same chip and optics would then be applicable to other commercial markets, such as continuous monitoring

during mechanical circulatory support, by adding a specialized continuous sample flow controller to the system.

7 REFERENCES

1 CA Warnes, et al., *Acc/aha 2008 guidelines for the management of adults with congenital heart disease: A report of the american college of cardiology/american heart association task force on practice guidelines (writing committee to develop guidelines on the management of adults with congenital heart disease).* Circulation, 2008. **118**(23): p. e714-833.

2 AJ Marelli, et al., *Congenital heart disease in the general population - changing prevalence and age distribution.* Circulation, 2007. **115**(2): p. 163-172.

3 VL Roger, et al., *Heart disease and stroke statistics-2011 update a report from the american heart association.* Circulation. **123**(4): p. E18-E209.

4 NM Haines, et al., *Extracorporeal life support registry report 2008: Neonatal and pediatric cardiac cases.* Asaio Journal, 2009. **55**(1): p. 111-116.

5 Spinal cord injury facts and figures at a glance, 2010

6 O Hausmann, *Post-traumatic inflawing spinal cord injury.* Spinal Cord, 2003. **41**(7): p. 369-378.

7 V Kuman, A Abbas, and N Fausto, *Robbins & cotran pathologic basis of disease, 7th edition*. 7 ed. 2004: Saunders. 1552.

8 JW Kirklin and BG Barratt-Boyes, *Hypothermia, circulatory arrest, and cardiopulmonary bypass. In: Kirklin jw, barrett-boyes bg (eds) cardiac surgery.* 2nd ed. Cardiac surgery, ed. JW Kirklin and BG Barratt-Boyes. 1993, New York. 61-128.

9 FD Moore, KG Warner, and S Assousa, *The effects of complement activation during cardiopulmonary bypass: Attenuation by hypothermia, heparin, and hemodilution.* Ann Surg, 1988. **208**: p. 95-103.

10 S Westaby, *Organ dysfunction after cardiopulmonary bypass: A systemic inflammatory reaction initiated by the extracorporeal circuit.* Intensive Care Med, 1987. **13**: p. 89-95.

11 R Ascione, et al., *Inflammatory response after coronary revascularization with or without cardiopulmonary bypass.* Annals of Thoracic Surgery, 2000. **69**(4): p. 1198-1204.

12 LH Edmunds, *Inflammatory response to cardiopulmonary bypass.* Annals of Thoracic Surgery, 1998. **66**(5): p. S12-S16.

13 E Fosse, TE Mollnes, and B Ingvaldsen, *Complement activation during major operations with or without cardiopulmonary bypass.* Journal of Thoracic and Cardiovascular Surgery, 1987. **93**(6): p. 860-866.

14 TE Mollnes, *Complement and biocompatibility.* Vox Sanguinis, 1998. **74**: p. 303-307.

15 JA Carr and N Silverman, *The heparin-protamine interaction - a review.* Journal of Cardiovascular Surgery, 1999. **40**(5): p. 659-666.

16 SA Rollins, et al., *Role of porcine p-selectin in complement-dependent adhesion of human leukocytes to porcine endothelial cells.* Transplantation, 2000. **69**(8): p. 1659-1667.

17 MC Seghaye, et al., *Complement activation during cardiopulmonary bypass in infants and children - relation to postoperative multiple system organ failure.* Journal of Thoracic and Cardiovascular Surgery, 1993. **106**(6): p. 978-987.

18 P Gessler, et al., *Inflammatory response and neurodevelopmental outcome after open-heart surgery in children.* Pediatric Cardiology, 2009. **30**(3): p. 301-305.

19 DE Chenoweth, et al., *Complement activation during cardiopulmonary bypass: Evidence for generation of c3a and c5a anaphylatoxins.* New England Journal of Medicine, 1981. **304**(9): p. 497-503.

20 M Fung, et al., *Inhibition of complement neutrophil, and platelet activation by an anti-factor d monoclonal antibody in simulated cardiopulmonary bypass circuits.* Journal of Thoracic and Cardiovascular Surgery, 2001. **122**(1): p. 113-122.

21 JK Kirklin, EH Blackstone, and JW Kirklin, *Intracardiac surgery in infants under age 3 months: Incremental risk factors for hospital mortality.* American Journal of Cardiology, 1981. **48**: p. 500-506.

22 A Undar, et al., *Anesthetic induction with ketamine inhibits platelet activation before, during, and after cardiopulmonary bypass in baboons.* Artificial Organs, 2004. **28**(10): p. 959-962.

23 ME Lull, et al., *Plasma biomarkers in pediatric patients undergoing cardiopulmonary bypass.* Pediatric Research, 2008. **63**(6): p. 638-644.

24 A Undar, et al., *Design and performance of a physiologic pulsatile flow neonate-infant cardiopulmonary bypass system.* Asaio Journal, 1996. **42**(5): p. M580-M583.

25 A Undar and CD Fraser, *Anti-factor d monoclonal antibody, pulsatile flow and cardiotomy suction during cardiopulmonary bypass.* European Journal of Cardio-Thoracic Surgery, 2002. **22**(2): p. 330-331.

26 A Undar, et al., *The type of aortic cannula and membrane oxygenator affect the pulsatile waveform morphology produced by a neonate-infant cardiopulmonary bypass system in vivo.* Artificial Organs, 1998. **22**(8): p. 681-686.

27 AEM Mautes, et al., *Vascular events after spinal cord injury: Contribution to secondary pathogenesis.* Physical Therapy, 2000. **80**(7): p. 673-687.

28 JC Fleming, et al., *The cellular inflammatory response in human spinal cords after injury*. Brain, 2006. **129**: p. 3249-3269.

29 M Oudega, et al., *Long-term effects of methylprednisolone following transection of adult rat spinal cord.* European Journal of Neuroscience, 1999. **11**(7): p. 2453-2464.

30 PG Popovich, et al., *Depletion of hematogenous macrophages promotes partial hindlimb recovery and neuroanatomical repair after experimental spinal cord injury.* Experimental Neurology, 1999. **158**(2): p. 351-365.

31 PG Popovich and TB Jones, *Manipulating neuroinflammatory reactions in the injured spinal cord: Back to basics.* Trends in Pharmacological Sciences, 2003. **24**(1): p. 13-17.

32 PG Popovich, P Wei, and BT Stokes, *Cellular inflammatory response after spinal cord injury in sprague-dawley and lewis rats.* Journal of Comparative Neurology, 1997. **377**(3): p. 443-464.

33 C Profyris, et al., *Degenerative and regenerative mechanisms governing spinal cord injury*. Neurobiology of Disease, 2004. **15**(3): p. 415-436.

34 MB Bracken, et al., *A randomized, controlled trial of methylprednisolone or naloxone in the treatment of acute spinal-cord injury - results of the 2nd national acute spinal-cord injury study.* New England Journal of Medicine, 1990. **322**(20): p. 1405-1411.

35 A Gorio, et al., *Methylprednisolone neutralizes the beneficial effects of erythropoietin in experimental spinal cord injury.* Proceedings of the National Academy of Sciences of the United States of America, 2005. **102**(45): p. 16379-16384.

36 WH Donovan, et al., *Intravenous infusion of 4-ap in chronic spinal cord injured subjects.* Spinal Cord, 2000. **38**(1): p. 7-15.

37 JA Halter, et al., *Intrathecal administration of 4-aminopyridine in chronic spinal injured patients.* Spinal Cord, 2000. **38**(12): p. 728-732.

38 RD Mainwaring, JJ Lamberti, and TE Hugli, *Complement activation and cytokine generation after modified fontan procedure.* Annals of Thoracic Surgery, 1998. **65**(6): p. 1715-1720.

39 CA Dinarello, *The interleukin-1 family - 10 years of discovery.* Faseb Journal, 1994. **8**(15): p. 1314-1325.

40 F Qiao, et al., *Complement plays an important role in spinal cord injury and represents a therapeutic target for improving recovery following trauma.* American Journal of Pathology, 2006. **169**(3): p. 1039-1047.

41 JK Dyer, JA Bourque, and JD Steeves, *The role of complement in immunological demyelination of the mammalian spinal cord.* Spinal Cord, 2005. **43**(7): p. 417-425.

42 CX Wang, JA Olschowka, and JR Wrathall, *Increase of interleukin-1 beta mrna and protein in the spinal cord following experimental traumatic injury in the rat.* Brain Research, 1997. **759**(2): p. 190-196.

43 L Shi, et al., *Peripheral inflammation modifies the effect of intrathecal il-1 beta on spinal pge(2) production mainly through cyclooxygenase-2 activity. A spinal microdialysis study in freely moving rats.* Pain, 2006. **120**(3): p. 307-314.

44 YL Lai, et al., *Sampling and analysis of cerebrospinal fluid for chronic studies in awake rats.* J Appl Physiol, 1983. **54**(6): p. 1754-1757.

45 H Bouman and T Van Wimmersma Gredianus, *A rapid and simple cannulation technique for repeated sampling of cerebrospinal fluid in freely moving rats.* Brain Research Bulletin, 1979. **4**(4): p. 575-577.

46 G Silverberg, et al., *Amyloid and tau accumulation precede csf production decline in normal aging.* Cerebrospinal Fluid Research, 2009. **6**(Suppl 1): p. S38.

47 M Tuna, et al., *Effect of anti-rat interleukin-6 antibody after spinal cord injury in the rat: Inducible nitric oxide synthase expression, sodium- and potassium-activated, magnesium-dependent adenosine-5 '-triphosphatase and superoxide dismutase activation, and ultrastructural changes.* Journal of Neurosurgery, 2001. **95**(1): p. 64-73.

48 I Pineau and S Lacroix, *Proinflammatory cytokine synthesis in the injured mouse spinal cord: Multiphasic expression pattern and identification of the cell types involved.* Journal of Comparative Neurology, 2007. **500**(2): p. 267-285.

49 HJ Muller-Eberhard, *Complement.* Annual Review of Biochemistry, 1969. **38**(1): p. 389-414.

50 PH Pfeifer, MS Kawahara, and TE Hugli, *Possible mechanism for in vitro complement activation in blood and plasma samples: Futhan/edta controls in vitro complement activation.* Clin Chem, 1999. **45**(8): p. 1190-1199.

51 K Sato, et al., *Microchip-based enzyme-linked immunosorbent assay (microelisa) system with thermal lens detection.* Lab on a Chip, 2004. **4**(6): p. 570-575.

52 XH Cheng, et al., *A microfluidic device for practical label-free cd4+t cell counting of hiv-infected subjects.* Lab on a Chip, 2007. **7**(2): p. 170-178.

53 EP Kartalov, et al., *High-throughput multi-antigen microfluidic fluorescence immunoassays.* Biotechniques, 2006. **40**(1): p. 85-90.

54 KC Ahn, et al., *High-throughput automated luminescent magnetic particle-based immunoassay to monitor human exposure to pyrethroid insecticides.* Analytical Chemistry, 2007. **79**(23): p. 8883-8890.

55 A Bhattacharyya and CM Klapperich, *Design and testing of a disposable microfluidic chemiluminescent immunoassay for disease biomarkers in human serum samples.* Biomedical Microdevices, 2007. **9**(2): p. 245-251.

56 HX Wang, et al., *Microfluidic immunosensor based on stable antibody-patterned surface in pmma microchip.* Electrochemistry Communications, 2008. **10**(3): p. 447-450.

57 AC Barton, F Davis, and SPJ Higson, *Labeless immunosensor assay for prostate specific antigen with picogram per milliliter limits of detection based upon an ac impedance protocol.* Analytical Chemistry, 2008. **80**(16): p. 6198-6205.

58 HA Engstrom, PO Andersson, and S Ohlson, *A label-free continuous total-internal-reflection-fluorescence-based immunosensor.* Analytical Biochemistry, 2006. **357**(2): p. 159-166.

59 MG Roper, et al., *Microfluidic chip for continuous monitoring of hormone secretion from live cells using an electrophoresis-based immunoassay.* Analytical Chemistry, 2003. **75**(18): p. 4711-4717.

60 S Aoyagi, et al., *A new reagentless immunosensor for measuring igg concentration in human plasma based on fluorescence-enhancement immunoassay.* The Japanese Society for Artificial Organs, 2002. **5**: p. 60-63.

61 S Yang, A Undar, and JD Zahn, *Continuous cytometric bead processing within a microfluidic device for bead based sensing platforms.* Lab on a Chip, 2007. **7**: p. 588-595.

62 N Pamme, *Magnetism and microfluidics.* Lab on a Chip, 2006. **6**(1): p. 24-38.

63 J Do and CH Ahn, *A polymer lab-on-a-chip for magnetic immunoassay with on-chip sampling and detection capabilities.* Lab on a Chip, 2008. **8**(4): p. 542-549.

64 JW Choi, et al., *An integrated microfluidic biochemical detection system for protein analysis with magnetic bead-based sampling capabilities.* Lab on a Chip, 2002. **2**(1): p. 27-30.

65 M Herrmann, T Veres, and M Tabrizian, *Enzymatically-generated fluorescent detection in micro-channels with internal magnetic mixing for the development of parallel microfluidic elisa.* Lab on a Chip, 2006. **6**(4): p. 555-560.

66 SA Peyman, A Iles, and N Pamme, *Rapid on-chip multi-step (bio)chemical procedures in continuous flow - manoeuvring particles through co-laminar reagent streams.* Chemical Communications, 2008(10): p. 1220-1222.

67 BD_Biosciences, *Bd cytometric bead array (cba), human anaphylatoxin kit instruction manual*.

68 SS Shevkoplyas, et al., *The force acting on a superparamagnetic bead due to an applied magnetic field.* Lab on a Chip, 2007. **7**(10): p. 1294-1302.

69 DC Duffy, et al., *Rapid prototyping of microfluidic systems in poly(dimethylsiloxane).* Analytical Chemistry, 1998. **70**(23): p. 4974-4984.

70 YN Xia and GM Whitesides, *Soft lithography.* Annual Review of Materials Science, 1998. **28**: p. 153-184.

71 K Aran, LA Sasso, and JD Zahn, *Irreversible, direct bonding of nanopourous polymer membranes to pdms or glass microdevices.* Lab on a Chip, 2010. **10**(5): p. 548-552.

72 Bio-Rad, in *Bio-Plex Pro Assays, Cytokine, Chemokine, and Growth Factors, Instruction Manual*.

73 YJ Kang, et al., *A highly accurate and consistent microfluidic viscometer for continuous blood viscosity measurement.* Artificial Organs. **34**(11): p. 944-949.

74 One hundred fifth congress of the united states of america first session, act to amend the federal food, drug, and cosmetic act and the public health service act to improve the regulation of food, drugs, devices, and biological products, and for other purposes, 1997